國 立 交 通 大 學

電子工程學系 電子研究所碩士班

碩 士 論 文

適用於高速移動的無線都會網路正交分頻多工空時區塊碼干擾消除器之設計

Design of OFDM STBC Interference Canceller for High-Mobility Wireless Metropolitan Area Network

研 究 生：張為凱

指導教授：周世傑 博士

中 華 民 國 九 十 九 年 十 月

適用於高速移動之無線都會網路空時區塊碼正交分頻多工干擾消除器設計

Design of STBC OFDM Interference Canceller for High-Mobility Wireless Metropolitan Area Network

研究生：張為凱　　Student: Wei-Kai Chang

指導教授：周世傑 博士　　Advisor: Dr. Shye-Jye Jou

國 立 交 通 大 學

電 子 工 程 學 系

碩 士 論 文

A Thesis

Submitted to Department of Electronics Engineering & Institute of Electronics

College of Electrical and Computer Engineering

National Chiao Tung University

in Partial Fulfillment of the Requirements

for the Degree of Master

in

Electronics Engineering

October 2010

HsinChu, Taiwan, Republic of China

中華民國九十九年十月

適用於高速移動之無線都會網路空時區塊碼正交分頻多工干擾消除器設計

研究生：張為凱　　指導教授：周世傑 博士

國立交通大學

電子工程學系 電子研究所碩士班

摘要

近年來，時空區塊碼(space-time block code; STBC)已被證實可以提供高編碼率及好的效能。在多根傳輸天限的正交多頻分工(orthogonal frequency-division multiplexing; OFDM）的系統應用中，時空區塊碼可增加分集增益(diversity gain)而且也被IEEE802.16e/m 規格支援。但是時空區塊碼對於單一編碼字元時間間隔內的通道時域變化非常敏感，這些變化將使得單一邊碼字元內的符元資料互相干擾；而且時變性多路徑通道也會在正交多頻分工系統的次載波間引發正交多頻分工次載波間干擾(Inter-carrier Interference;ICI)效應。這些干擾雜訊會破壞空時區塊碼與正交分頻多工系統結合之系統應用（STBC-OFDM systems）的性能，因此我們必須一種空時區塊碼正交分頻多工干擾消除器才能在無法取得詳細的通道狀態資訊（channel state information; CSI）的狀況下達到更好的效能。

這篇論文將提出一個可適用於高速移動環境中兩根傳送天線與一根接收天線之空時區塊碼與正交分頻多工系統結合之系統的干擾消除器。此空時區塊碼正交分頻多工干擾消除器的設計是基於一套現存 IEEE802.16e 規格的接收器，但是它也可以輕易的修改為 IEEE802.16e 規格。設計的目標是在高達時速 360 公里的移動環境中提供效能的

改善，我們將提出的設計與一套被研究過的兩階段通道估測器(two-stage channel estimator)搭配來展示效能，在時速240及360公里、訊噪比(signal to noise ratio;SNR)高於 15dB、16 正交振幅調變（16 quadrature amplitude modulation; 16-QAM）的環境中可減少位元錯誤率（bit error rate; BER）超過2倍。我們以 90 nm CMOS 製程實現此干擾消除器設計。總共需要 42,277 個邏輯閘，在 78.4MHz 的操作頻率與 1 V 工作電壓下，其功率消耗為 1.45 mW。干擾消除器設計中大約 61%的邏輯閘可以與現有的兩階段通道估測器共用，額外的負擔只占原先兩階段通道估測器的 4.9%

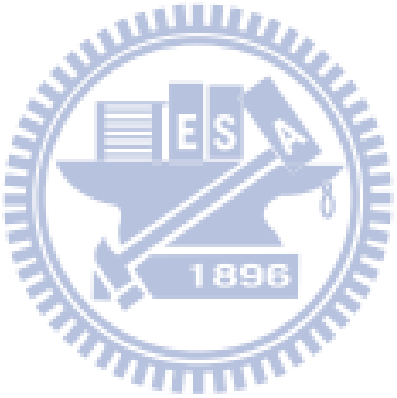

Design of STBC OFDM Interference Canceller for High-Mobility Wireless Metropolitan Area Network

Student：Wei-Kai, Chang Advisor：Dr. Shyh-Jye, Jou

Department of Electronics Engineering & Institute of Electronics

National Chiao Tung University

Abstract

In recent years, space time block code (STBC) has been shown to give high code rate and good performance. It is suggested to be applied in an orthogonal frequency division multiplex (OFDM) system since OFDM system with multiple antennas can provide better communication performance by exploiting transmit diversity and it was also supported by IEEE 802.16e/m standard. Nevertheless, STBC is sensitive to the temporal channel variation inside one code word which results in the symbols inside one codeword interferes with each other. Also, time-varying multipath channel introduces intercarrier interference (ICI) among OFDM subcarriers. These interference noises degrade STBC-OFDM system performance. Hence, an STBC interference cancellation scheme is required for better performance when the detailed channel statistics information (CSI) variation is unavailable.

This thesis proposes an STBC interference canceller for any STBC-OFDM systems with two transmit antenna and one receive antenna in mobile environment. The proposed STBC interference canceller is applied in an existed IEEE802.16e STBC-OFDM receiver and can easily be adapted into IEEE802.16m STBC-OFDM receiver, too. The proposed design aims to provide performance improvement under the vehicle speed up to 360 km/hr. The

performances have been demonstrated through the simulation of the proposed design with a previously proposed two-stage channel estimator. At vehicle speed of 240 and 360 km/hr and signal to noise ratio (SNR) over 15dB for 16 quadrature amplitude modulation (16QAM), the proposed design can provide more than 2 times bit error rate (BER) improvement. The proposed design is implemented in 90 nm CMOS technology. The gate count is 42,277 and the power dissipation is 1.45 mW at 78.4 MHz operation frequency from a supply voltage 1V. About 61% gates of our proposed STBC interference canceller are shared with the existed two-stage channel estimator design, and the overhead is only 4.9%.

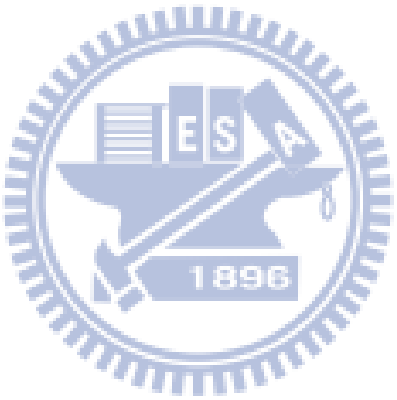

誌　謝

隨著這份研究的完成我獲得了交大電子工程碩士學位，研發替代役也順利應徵上人人稱羨的聯發科技，離鄉背井六年的求學生涯就此告一段落。這段旅途的圓滿結局泰半得歸功於一路上諸多貴人幫助，因為要感激的人實在太多了，光用「謝天」二字籠統帶過會經不起良心譴責而輾轉難眠。

首先要感謝我的指導老師周教授世傑先生，感謝他在 2008 年碩士班推甄時接受我的毛遂自薦，並且提供我優渥舒適的研究環境和研究方向，讓我得依自己的興趣精進通訊演算法技能並同時兼顧電路設計的基本功夫。在學業課題外，周老師的教誨也啟發我讓我以更積極、樂觀的態度去體驗和學習待人接物的道理。

接著要感謝帶領我研究的 MOMO 學姊，多虧學姊胼手胝足建立了通道估計的電路硬體及完善的軟體模擬平台，我的構想才得以發揮與驗證；在我研究遭遇瓶頸搜索枯腸時，學姊也願意犧牲時間幫忙我除蟲和傷腦筋。

也謝謝諸位實驗室的前輩們，小肥、小胖、儷蓉、大大、麥哥、阿賢、銘銓、范姜、嘉文、亦緯、代暘、淳淳哥等，學校裡各式各樣難解的疑難雜症在他們熱心幫忙下都可迎刃而解。也感謝同儕朋友和學弟妹的情義相挺，以樂、TMC、雅雪、烏克蘇、福鈞、育瑞、紹丞、佳怡、Juii 等。

最後還要感謝我最親愛的家人以及女友恩立長久以來的照顧與支持，讓我可以徜徉書海醉心研究而無後顧之憂，謹將所有的成就和榮耀獻給他們。

張為凱

謹誌於 新竹

2010 年 10 月

Contents

List of Figures

List of Tables

Chapter 1 Introduction

1.1 Overview of IEEE 802.16e/m OFDM systems

Wireless Metropolitan Area Network (WiMAN), allowing end-users to travel throughout a hot zone cell without losing connectivity, has been an very important technique in wireless communication. The services provide portability and mobility to make users more convenient to access information. For the high quality service, the channel capacity seems more important for WiMAN, therefore, the error correcting capability is a great issue in WiMAN. WiMAN is defined by IEEE 802.16 Working Group on Worldwide Internet access (BWA) standards and commercially known as Worldwide Interoperability for Microwave Access (WiMAX) which defines broadband Internet access from fixed or mobile devices via antennas.

IEEE 802.16e standard [1] was released in 2005 and is often referred to as mobile WiMAX. It is an extension of IEEE802.16-2004 for providing high data rate transmission and mobility of WMAN. It enables mobile speed up to 120 km/hr, but also backward compatible to support the fixed mode in IEEE 802.16-2004. Operation in mobile mode is limited to the license bands between 2-6 GHz. It is based on an OFDMA technique to support multiple access scheme and multiple-input multiple output (MIMO) systems over multipath fading channels.

IEEE 802.16m standard [2] is an updated version of IEEE 802.16e. It is also fully backward compatible to support the older IEEE 802.16 standards, and targets to attract new operators that starts the deployment from 2012. Note that the enabled mobile speed is increased to 350 km/hr. The other major differences between 802.16e and 802.16m are discussed in Section3.1.4.

In this thesis design and implementation of STBC interference canceller for high mobility WiMAN is proposed. The implementation uses IEEE802.16e as a test vehicle and can also be adopted in IEEE802.16m application.

1.2 Motivation

IEEE 802.16e/m systems effectively provide wireless transmission of data using a variety of transmission modes from point-to-multipoint links to portable and fully mobile internet access. The research of IEEE 802.16e/m systems have gained more and more interest and become the world wide topic. However, in mobile wireless communication, the channel often varies rapidly, which results in a large Doppler spread, particularly when the mobile station (MS) moves at a vehicular speed. A fundamental phenomenon that makes credible wireless transmission expensive and difficult is time-varying multipath channels. In order to improve the transmission quality in fast and selective fading channels, transmit diversity is an effective technology for reducing fading effect in mobile wireless communication, especially when receive diversity is expensive or impractical to acquire.

In recent years, space time block code (STBC) has been shown to give high code rate and good performance. It is suggested to be applied in an OFDM system since OFDM system with multiple antennas can provide better communication performance by exploiting transmit diversity and it was also supported by IEEE 802.16e/m standard. Nevertheless, STBC is sensitive to the temporal channel variation inside one code word which results in the symbols inside one codeword interferes with each other. Also, time-varying multipath channel introduce intercarrier interference (ICI) among OFDM subcarriers. These interference noises degrade STBC-OFDM system performance. Hence, an STBC interference cancellation scheme is required for better performance when the detailed channel statistics information (CSI) variation is unavailable.

In this thesis, we focus on the design and development of an STBC interference canceller applied in an IEEE 802.16e down link baseband receiver. The proposed algorithm and hardware architecture are proposed to present an efficient and low-overhead solution for any conventional STBC-OFDM system.

1.3 Thesis Organization

The rest of this thesis is organized as follows. Chapter 2 introduces the principle of STBC OFDM and formulates its interference noise components introduced by time-variant channels. Chapter 3 presents the algorithm design and its simulation results. The goal of the proposed design is to integrate with an recently published two-stage STBC-OFDM channel estimator [3] to improve system performance at high-mobility and high-QAM constellation applications. In Chapter 4, an efficient architecture is provided to keep high performance without increasing hardware overhead. Finally, Chapter 5 is the conclusion.

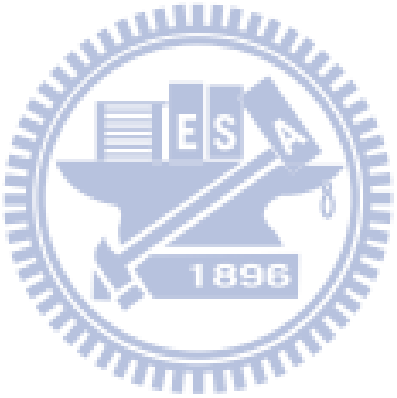

Chapter 2 Interference of STBC-OFDM Systems in Wireless Mobile Environment

MIMO-ODFM technique employs multiple antennas at the transmitter or receiver to increase diversity gain and improve system performance without additional bandwidth or transmit power. But in modern wireless mobile applications, receiver diversity is considered too costly to be implemented. The concept of space-time block code (STBC) provides a very efficient method to exploit transmit diversity. In recent years, STBC-OFDM has been adopted in 802.16e/m to support high speed applications.

STBC requires the channel between each transmit-receive antenna pair to be constant over the symbol periods inside 1 code word. However, this assumption rarely holds in highly mobile applications. Time domain channel variation results in several kinds of interference noise during decoding and impact system performance. In this chapter, we will derive these interference noises and demonstrate their effects on system performance through simulation.

2.1 STBC-OFDM Systems under Quasi-Static Channel

We begin this chapter with the assumption that the channels do not vary over a STBC code word period, it is also known as “quasi-static condition”. Fig.2.1 is a conventional OFDM system having transmit diversity.

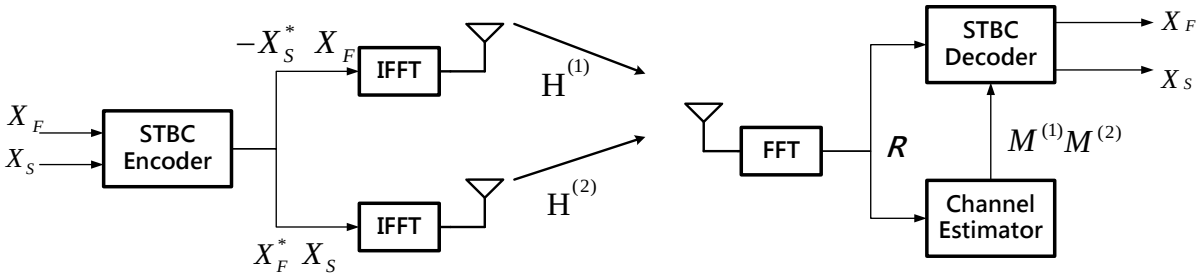

Fig.2.1 Conventional STBC-OFDM system with quasi-static channel

2.1.1 STBC Encoding

Among various STBC scheme that has been studied, Alamouti coding scheme is the most popular and practical one [4]. This scheme requires 2 transmit antenna and 1 receive antenna as shown in Fig.2.1. Each block code word occupies the length of 2 symbol interval, or 1 "time slot." 2 OFDM symbols, and , are encoded and transmit from different antenna in the manner described in Table 2.1, where is the subcarrier index , N is the total number of subcarriers ,and the superscript * stands for complex conjugate.

Table 2.1 Transmit symbols of Alamouti STBC encoding scheme

		Transmit Antenna	
		1st Antenna	2nd Antenna
One time slot duration	1st Symbol Interval	$\mathbf{X}_F$	$\mathbf{X}_S$
	2nd Symbol Interval	$-\mathbf{X}_S^*$	$\mathbf{X}_F^*$

2.1.2 STBC Decoding

The channel frequency response between the first transmit antenna and receive antenna at the ts -th time slot is denoted as $\mathrm{H}_{ts}^{(1)}[k]$ and the other one is denoted as $\mathrm{H}_{ts}^{(2)}[k]$. Within this time slot, the 1st and 2nd received OFDM symbols, $R_{ts}[1,k]$ and $R_{ts}[1,k]$, can be expressed as

$$\begin{aligned} R_{ts}[1,k] &= \mathrm{H}_{ts}^{(1)}[k]X_F[k] + \mathrm{H}_{ts}^{(2)}[k]X_S[k] + Z_{ts}[1,k] \\ R_{ts}[2,k] &= -\mathrm{H}_{ts}^{(1)}[k]\left(X_S[k]\right)^* + \mathrm{H}_{ts}^{(2)}[k]\left(X_F[k]\right)^* + Z_{ts}[2,k] \end{aligned} \tag{2.1}$$

for $k \in \mathbf{Q} \cup \mathbf{J}$, where $\mathbf{Q}$ and $\mathbf{J}$ denote the set of data and pilot subcarrier indices, respectively,

and $Z_{ts}[1,k]$ and $Z_{ts}[2,k]$ are the uncorrelated additive white Gaussian noise (AWGN) with zero-mean and variance σ_z^2.

To demonstrate decoding process clearly, we reformulate (2.1) as below.

$$\underbrace{\begin{bmatrix} R_{ts}[1,k] \\ (R_{ts}[2,k])^* \end{bmatrix}}_{\mathrm{Y_{ts}}[k]} = \underbrace{\begin{bmatrix} \mathrm{H}_{ts}^{(1)}[k] & \mathrm{H}_{ts}^{(2)}[k] \\ \left(\mathrm{H}_{ts}^{(2)}[k]\right)^* & -\left(\mathrm{H}_{ts}^{(1)}[k]\right)^* \end{bmatrix}}_{\mathrm{A}_{ts}[k]} \underbrace{\begin{bmatrix} X_F[k] \\ X_S[k] \end{bmatrix}}_{\mathrm{X}[k]} + \underbrace{\begin{bmatrix} Z[1,k] \\ (Z[2,k])^* \end{bmatrix}}_{\mathrm{Z_{ts}}[k]} \tag{2.2}$$

To perform simple Alamouti decoding, we multiplying $\mathrm{A}_{ts}^H[k]$ with received signals and the 2 symbols in $\mathrm{X}[k]$ are decoupled from each other:

$$\begin{aligned} \mathrm{A}_{ts}^H[k]\mathrm{Y_{ts}}[k] &= \mathrm{A}_{ts}^H[k]\mathrm{A}_{ts}[k]\mathrm{X_{ts}}[k] + \mathrm{A}_{ts}^H[k]\mathrm{Z_{ts}}[k] \\ &= \sigma_{ts}[k]\mathrm{X_{ts}}[k] + \mathrm{A}_{ts}^H[k]\mathrm{Z_{ts}}[k] \\ \sigma_{ts}[k] &\triangleq \left|\mathrm{H}_{ts}^{(1)}[k]\right|^2 + \left|\mathrm{H}_{ts}^{(2)}[k]\right|^2 \end{aligned} \tag{2.3}$$

where superscript "*H*" stands for Hermitian transpose. Based on the latest estimated channel frequency response $M^{(1)}$ and $M^{(2)}$, the decision of 2 transmitted symbol can be made independently by the following equations

$$\begin{aligned} X_F[k] &= \frac{1}{\zeta_{ts}[k]}\left(\left(M_{ts}^{(1)}[k]\right)^* R_{ts}[1,k] + M_{ts}^{(2)}[k]\left(R_{ts}[2,k]\right)^*\right) \\ X_S[k] &= \frac{1}{\zeta_{ts}[k]}\left(\left(M_{ts}^{(2)}[k]\right)^* R_{ts}[1,k] - M_{ts}^{(1)}[k]\left(R_{ts}[2,k]\right)^*\right) \\ \zeta_{ts}[k] &\triangleq \left|M_{ts}^{(1)}[k]\right|^2 + \left|M_{ts}^{(2)}[k]\right|^2 \end{aligned} \tag{2.4}$$

2.2 Time-variant Multipath Channel and ICI Effect of OFDM Systems

2.2.1 Time-variant Multipath Channel

In mobile wireless environment, multipath channels are usually time-variant. Although the degree of channel variation over an sampling period decrease as data rate becomes higher, the time variation of a fading channel over an OFDM symbol interferes the orthogonality between subcarriers. This undesired effect in known as intercarrier interference (ICI). As the vehicle speed increases, it introduces Doppler spread and increases the error floor.

Without loss of generality, we consider an single-input-single-output (SISO) OFDM system that has only one transmit antenna. Let $X[k]$ be the data symbol transmitted through the k-th subcarrier for an OFDM symbol. Then after N-point inverse fast Fourier transform (IFFT) modulation and appending cyclic prefix with length N_g, the transmitted time domain data symbol at time q is denoted as

$$x[q] = \frac{1}{N}\sum_{k=0}^{N-1} X[k] e^{j\frac{2\pi kq}{N}}, \quad for \;\; q = -N_g, -N_g+1, \cdots, N-1 \tag{2.5}$$

Assuming the multipath fading channel between the *i*-th transmit antenna and the receive antenna is made of L discrete paths, the received signal can be expressed as [4].

$$r[q] = \sum_{l=1}^{L} h_l[N_g + q]x[q-l] + z[N_g + q] \tag{2.6}$$

where $h_l[b]$ and $z[b]$ represents the complex path gain for the l-th path and AWGN at time b respectively. By removing the cyclic prefix and taking the fast Fourier transform (FFT), the demodulated signal in frequency domain is given by

$$R[k] = \sum_{m=0}^{N-1}\sum_{l=1}^{L}\left\{ X[m]\left(\frac{1}{N}\sum_{q=0}^{N-1} h_l[q] e^{j\frac{2\pi q(m-k)}{N}} \right) e^{-j2\frac{m}{N}\tau_l} \right\} + Z[k]$$
$$= \sum_{m=0}^{N-1} \mathrm{H}[k,m]X[m] + Z[k] \tag{2.7}$$

$$H[k,m] \triangleq \sum_{l=1}^{L}\left\{ e^{-j2\frac{m}{N}\tau_l} \left(\frac{1}{N}\sum_{q=0}^{N-1} h_l[q] e^{j\frac{2\pi q(m-k)}{N}} \right) \right\} \tag{2.8}$$

where $H[k,m]$ represents the frequency domain channel coefficient between the m-th transmitted subcarrier to the k-th received subcarrier, $Z[k]$ is the FFT of AWGN, τ_l denotes the delay of the l-th path ,and $m = 0,1,2,\cdots,N\text{-}1$.

The significance of channel variation can be measured as the correlation of 2 channel impulse response samples separated by an given time ρ, defined as $\varsigma(\rho) = E\left\{ h_l[q+\rho] h_l^*[q] \right\}$. According to the studies of [5], the correlation function and vehicle speed has the following relation

$$\varsigma(\rho) = J_0(2\pi f_d \rho)$$
$$f_d \triangleq \left(\frac{V_E}{V_c} \right) \cdot f_c \tag{2.9}$$

where f_d is the Doppler frequency, V_E represents vehicle speed, V_c stands for light speed, f_c denotes carrier frequency, and $J_0(x)$ is the zeroth-order Bessel function of the first kind.

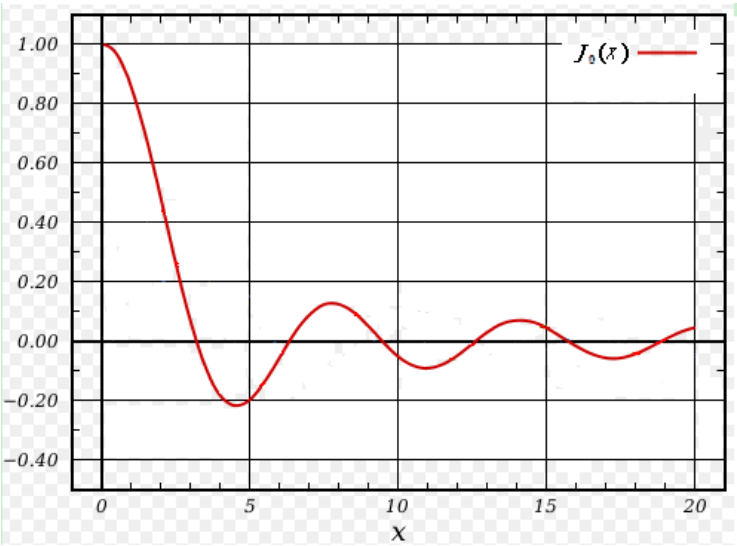

Fig2.2 Zero-th order Bessel function of the first kind

And the spectral density of $\varsigma(\rho)$ is the renowned "Jakes model". It can be observed from Fig.2.2 that given a fixed carrier frequency, the absolute value of $\varsigma(\rho)$ decreases when vehicle speed increases. Therefore, the temporal channel variation becomes more random and abrupt in high speed environment. Rapid temporal channel variation results in Doppler spread effect in frequency domain described by (2.10), where $P_J(f)$ stands for the power spectral density at frequency f.

$$P_J(f)=\begin{cases}\dfrac{1}{\pi f_d}\dfrac{1}{\sqrt{1-\left(\dfrac{f}{f_d}\right)^2}} & \text{, if } |f|<f_d \\ 0 & \text{, elsewhere}\end{cases} \tag{2.10}$$

In OFDM systems, Doppler spread effect causes ICI between neighboring subcarriers. The performance loss due to the ICI becomes significant as the carrier frequency, OFDM block interval, and vehicle speed increase.

2.2.2 ICI effect

The channel matrix H can be simplified as

$$H[k,m]=\begin{cases}\sum_{l=0}^{L-1}\bar{h}_l[k]e^{-j2\frac{k}{N}\tau_l} & ;\text{ if } k=m\\ \sum_{l=0}^{L-1}\left\{e^{-j2\frac{m}{N}\tau_l}\left(\frac{1}{N}\sum_{q=0}^{N-1}h_l[q]e^{j\frac{2\pi q(m-k)}{N}}\right)\right\} & ;\text{ if } k\neq m\end{cases} \tag{2.11}$$

$$\bar{h}_l \triangleq \frac{1}{N}\sum_{q=0}^{N-1}h_l[N_g+q] \tag{2.12}$$

where $\bar{h}_l$ is time average of the l-th complex path gain over the effective duration of an OFDM symbol interval. It should be note that the diagonal terms of H is the FFT of $\bar{h}_l$, and is equivalent to our desired channel frequency response. Those off-diagonal terms stands for the coupling coefficient between different subcarriers which results in ICI effect. For better comprehension, (2.7) can be rewritten as

$$R[k]=\mathrm{H}[k,k]X[k]+\underbrace{\sum_{\substack{m=0\\ m\neq k}}^{N-1}\mathrm{H}[k,m]X[m]}_{\text{ICI term}}+Z[k] \tag{2.13}$$

If our channel is time invariant, complex path gain at any time within the effect duration of an OFDM symbol is equal to $\bar{h}_l$, and it is easy to show that the off-diagonal terms of H becomes zero.

$$\begin{aligned}&h_l[N_g+p]=\bar{h}_l \quad \forall\left\{p\,\middle|\,0\le p\le(N-1)\right\}\\ &\Rightarrow\frac{1}{N}\sum_{q=0}^{N-1}h_l[q]e^{j\frac{2\pi q(m-k)}{N}}=\frac{\bar{h}_l}{N}\sum_{q=0}^{N-1}e^{j\frac{2\pi q(m-k)}{N}}=0 \quad \forall\ k\neq m\\ &\Rightarrow H[k,m]=0 \quad \forall\ k\neq m\end{aligned} \tag{2.14}$$

This implies that there is no ICI for time-invariant channel, and the received signal contains only the multiplicative distortion and AWGN. They can be easily dealt with one-tap equalizer and MAP detector. More detailed interpretations of h_l and H are provided in [4].

2.3 Interference Noise of STBC-OFDM Systems

For time-variant channels, channel variation between OFDM symbols become significant, and the "quasi-static condition" inside 1 STBC codeword period no longer holds. We have to consider the channel frequency response of the 2 symbol period respectively , and the OFDM system block diagram is modified as shown in Fig. 2.3., where $\mathrm{H}_{ts,b}^{(i)}$ denotes for the frequency domain channel matrix of i -th transmit antenna at the b -th symbol interval of the ts -th time slot, where $i \in \{1,2\}$, $b \in \{1,2\}$,and $ts = 1,2,3,\cdots$. The relationship of channel frequency response between different antenna and symbol interval is illustrated as Table. 2.2.

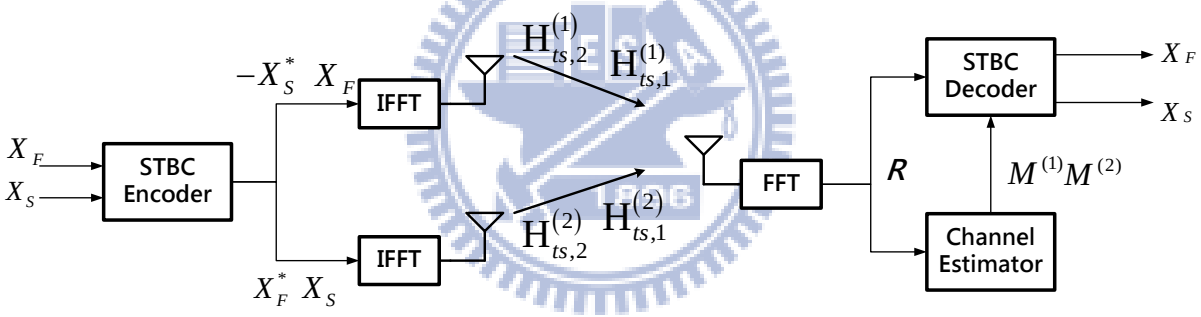

Fig.2.3 Conventional STBC-OFDM system with time-variant channel

Table 2.2 Frequency domain channel matrices of an STBC code word

		Transmit Antenna	
		1st Antenna	2nd Antenna
One time slot duration	1st Symbol Interval	$\mathrm{H}_{ts,1}^{(1)}$	$\mathrm{H}_{ts,1}^{(2)}$
	2nd Symbol Interval	$\mathrm{H}_{ts,2}^{(1)}$	$\mathrm{H}_{ts,2}^{(2)}$

As a result, the received signals of (2.2) becomes

$$\underbrace{\begin{bmatrix} R_{ts}[1,k] \\ \left(R_{ts}[2,k]\right)^{*} \end{bmatrix}}_{\mathrm{Y}_{ts}[k]} = \sum_{m=0}^{N-1} \underbrace{\begin{bmatrix} \mathrm{H}_{ts,1}^{(1)}[k,m] & \mathrm{H}_{ts,1}^{(2)}[k,m] \\ \left(\mathrm{H}_{ts,2}^{(2)}[k,m]\right)^{*} & -\left(\mathrm{H}_{ts,2}^{(1)}[k,m]\right)^{*} \end{bmatrix}}_{\mathrm{A}_{ts}[k,m]} \underbrace{\begin{bmatrix} X_F[m] \\ X_S[m] \end{bmatrix}}_{\mathrm{X}[m]} + \underbrace{\begin{bmatrix} Z_{ts}[1,k] \\ \left(Z_{ts}[2,k]\right)^{*} \end{bmatrix}}_{\mathrm{Z}_{ts}[k]} \quad (2.15)$$

Note that when the channels are in quasi-static condition, they are also time-invariant. So the off-diagonal terms of $\mathrm{H}_{ts,b}^{(i)}$ vanish and its diagonal terms is equivalent to $\mathrm{H}^{(i)}$ as shown in the following equations

$$\begin{aligned} &\mathrm{H}_{ts,1}^{(i)}[k,m] = \mathrm{H}_{ts,2}^{(i)}[k,m] = \begin{cases} \mathrm{H}_{ts}^{(i)}[k] & \text{if } k = m \\ 0 & \text{if } k \neq m \end{cases} \\ &\mathrm{A}_{ts}[k,m] = 0 \quad \forall\, k \neq m \\ &\mathrm{A}_{ts}[k] = \mathrm{A}_{ts}[k,k] \end{aligned} \quad (2.16)$$

and the simple Alamouti decoding in (2.4) offers maximum likelihood (ML) performance [6].

However, under time-varying channels, the off-diagonal terms of $\mathrm{H}_{ts,b}^{(i)}$ are not zero. If we separate those off-diagonal terms and time-varying components, equation (2.15) can be reformulated as

$$\mathrm{Y}_{ts}[k] = \overline{\mathrm{A}}_{ts}[k,k]\mathrm{X}[k] + \mathrm{A}_{ts,\Delta}[k,k]\mathrm{X}_{ts}[k] + \sum_{\substack{m=0 \\ m\neq k}}^{N-1} \overline{\mathrm{A}}_{ts}[k,m]\mathrm{X}[m] + \sum_{\substack{m=0 \\ m\neq k}}^{N-1} \mathrm{A}_{ts,\Delta}[k,m]\mathrm{X}_{ts}[m] \quad (2.17)$$

$$\overline{\mathrm{H}}_{ts}^{(i)}[k,m] \triangleq \frac{1}{2}\left(\mathrm{H}_{ts,1}^{(i)}[k,m]+\mathrm{H}_{ts,2}^{(i)}[k,m]\right),\ i\in\{1,2\}$$

$$\overline{\mathrm{A}}_{ts}\left[k,k\right] \triangleq \begin{bmatrix} \overline{\mathrm{H}}_{ts}^{(1)}[k,m] & \overline{\mathrm{H}}_{ts}^{(2)}\left[k,m\right] \\ \left(\overline{\mathrm{H}}_{ts}^{(2)}\left[k,m\right]\right)^{*} & -\left(\overline{\mathrm{H}}_{ts}^{(1)}\left[k,m\right]\right)^{*} \end{bmatrix}$$

$$\mathrm{A}_{ts,\Delta}\left[k,m\right] \triangleq \mathrm{A}_{\mathrm{ts}}\left[k,m\right]-\overline{\mathrm{A}}_{ts}\left[k,m\right] \qquad (2.18)$$

$$\mathrm{H}_{ts}^{(i)}[k]=\overline{\mathrm{H}}_{ts}^{(i)}[k,k]$$

$$\mathrm{A}_{ts}\left[k\right]=\overline{\mathrm{A}}_{ts}\left[k,k\right]$$

where $\overline{\mathrm{A}}_{ts}$ is composed of the averaged frequency domain channel matrix $\overline{\mathrm{H}}_{ts}^{(i)}$ over the *ts*-th time slot, and $\mathrm{A}_{ts,\Delta}$ is the variation part. If we apply the same Alamouti decoding technique using the above identity, then we have

$$\overline{\mathrm{A}}_{ts}^{H}\left[k,k\right]\mathrm{Y}_{ts}\left[k\right]=\sigma_{ts}[k]\mathrm{X}_{ts}[k]+\overline{\mathrm{A}}_{ts}^{H}\left[k,k\right]\left\{\alpha_{ts}\left[k\right]+\beta_{ts}\left[k\right]+\gamma_{ts}\left[k\right]+\zeta_{ts}\left[k\right]+\mathrm{Z}_{ts}\left[\mathrm{k}\right]\right\}$$
$$\sigma_{ts}[k]=\left|\overline{\mathrm{H}}_{ts}^{(1)}[k,k]\right|^{2}+\left|\overline{\mathrm{H}}_{ts}^{(2)}[k,k]\right|^{2} \qquad (2.19)$$

$$\alpha_{ts}\left[k\right] \triangleq \mathrm{A}_{ts,\Delta}[k,k]\mathrm{X}[k] \qquad \textbf{(CCI noise)} \qquad (2.20)$$

$$\beta_{ts}\left[k\right] \triangleq \sum_{\substack{m=0 \\ m\neq k}}^{N-1}\overline{\mathrm{A}}_{ts}\left[k,m\right]\mathrm{X}[m] \qquad \textbf{(averaged ICI noise)} \qquad (2.21)$$

$$\gamma_{ts}\left[k\right] \triangleq \sum_{\substack{m=0 \\ m\neq k}}^{N-1}\mathrm{A}_{ts,\Delta}\left[k,m\right]\mathrm{X}[m] \qquad \textbf{(variant ICI noise)} \qquad (2.22)$$

where $\alpha_{ts}\left[k\right]=\left[\alpha_{ts}\left[1,k\right]\ \ \alpha_{ts}\left[2,k\right]\right]^{\mathrm{T}}$ denotes the co-carrier interference (CCI), $\beta_{ts}\left[k\right]=\left[\beta_{ts}\left[1,k\right]\ \ \beta_{ts}\left[2,k\right]\right]^{\mathrm{T}}$ and $\gamma_{ts}\left[k\right]=\left[\gamma_{ts}\left[1,k\right]\ \ \gamma_{ts}\left[2,k\right]\right]^{\mathrm{T}}$ are the averaged and variant

part of ICI respectively. $\zeta_{ts}[k]=\left[\zeta_{ts}[1,k] \quad \zeta_{ts}[2,k]\right]^{\mathrm{T}}$ stands for the ICI from pilot subcarriers which we will discuss in Section 3.4.3. The presence of these 3 interference components in time-varying channels results in severe performance degradation.

It has been studied that CCI problem is more important than ICI problems, and simulation results provided in [7] suggests that the CCI power is larger than the ICI power by 7~8dB regardless of the channel variation rate.

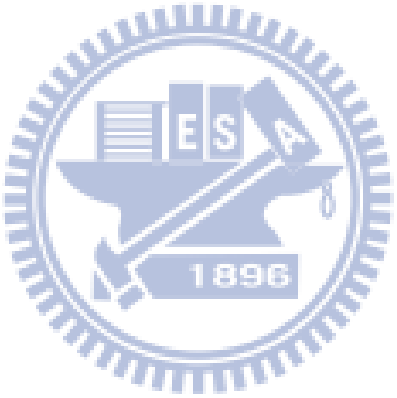

2.4 Proposed Decoding Flow

In order to mitigate the impact of CCI and ICI, various approaches have been studied [6-9]. In [7], an successive interference cancellation (SIC) and least squares (LS) method was proposed. In [9] the ML method was used to deal with CCI problem. In [6], a modified ML method was proposed to reduce the complexity of traditional ML method. Most of the previous works do not use Alamouti simple decoding technique and instead they use other sophisticated symbol detection methods. However, those symbol detection methods results in significant hardware overhead.

One design target of this thesis is to integrate the interference cancellation algorithm with an existing STBC-OFDM system [3]. Under limited clock cycle and hardware budget, our trade-off is to use simple Alamouti decoding technique for symbol detection and to focus on modeling interference noise components. Based on the method in [8], we use the following decoding flow:

(A) Channel Estimation

Estimate the channel frequency response without dealing with CCI and ICI noise to obtain $M_{ts}^{(1)}$ and $M_{ts}^{(2)}$ in Fig. 2.1.

(B) Initial Symbol Decision

Generate initial decision symbols using (2.4), denoted as $\mathrm{X}^{(0)}[k] = \begin{bmatrix} X_F^{(0)} & X_S^{(0)} \end{bmatrix}^T$.

(C) Interference Modeling

Approximate CCI and ICI based on channel estimation results, $M^{(1)}$ and $M^{(2)}$.

(D) Decision Symbol Updating

$$\mathrm{X}^{(\lambda+1)}[k] \leftarrow Dec\left\{\mathrm{Y}_{ts}[k] - \mathrm{CCI}^{(\lambda)} - \mathrm{ICI}^{(\lambda)}\right\} \tag{2.21}$$

where $Dec\{\cdot\}$ stands for simple Alamouti decoding using (2.4), $\mathrm{CCI}^{(\lambda)}$ and $\mathrm{ICI}^{(\lambda)}$ are the approximated CCI and ICI noise generated by $\mathrm{X}^{(\lambda)}[k]$, and λ denotes decoding iteration index.

(E) Iteration

Go back to step (C) until the simulated BER performance can no longer improved.

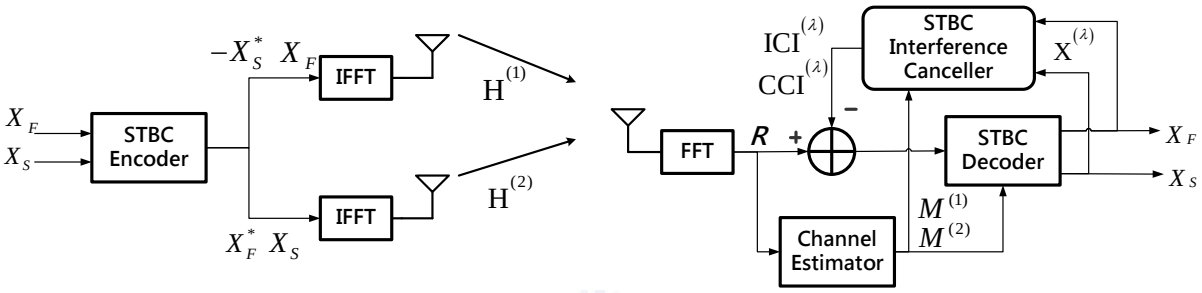

Fig.2.4 Proposed STBC-OFDM system with STBC interference canceller

The CCI and ICI modeling algorithm will be proposed in Chapter 3, and the proposed STBC OFDM system with STBC interference canceller is illustrated in Fig.2.4.

Chapter 3 STBC OFDM Interference Cancellation Algorithm

In Chapter 2 we derived the interference noise components of STBC-OFDM under time-variant channels, and a decoding flow was proposed to reduce the impact of interference noise during simple Alamouti decoding. In this Chapter, we propose an algorithm to model CCI and ICI components jointly, and then cancel these noises from received signals to provide a cleaner input for STBC decoding. We will start with an overview of the specification of our STBC-OFDM system, and introduce a robust two-stage channel estimator that has been proposed in [3] to provide an accurate channel frequency response. Then we propose the modeling algorithms for CCI and ICI respectively. Finally, the channel estimator and the proposed interference canceller will be integrated together, and some simulation results will show the improved system performance.

3.1 802.16e STBC OFDM System Specification

3.1.1 Frame Structure

In the licensed band, IEEE802.16e system can support time-division duplexing (TDD) or frequency division duplexing (FDD). The other license-exempt bands, only TDD should be used. Fig. 3.1 shows a frequently referred model of TDD mode frame structure. The frame structure includes the following elements. The first transmitted symbol of a frame is the preamble symbol which its elements are known at the receiver. Preamble is used for cell search, synchronization, and channel estimation. Following the preamble, the frame control header (FCH) with fixed size is transmitted for resource allocation such as subcarrier used, length of DL-MAP and DL_Frame_prefix, The quadrature phase shift keying (QPSK) modulation with code rate 1/2 and four repetitions is used for FCH transmission. DL_MAP and UL_MAP following FCH message for resource allocation of the various users in DL and UL data bursts. Transmit transition gap (TTG) is used to give base station (BS) and subscriber station (SS)

enough time to change from down link mode to up link mode.

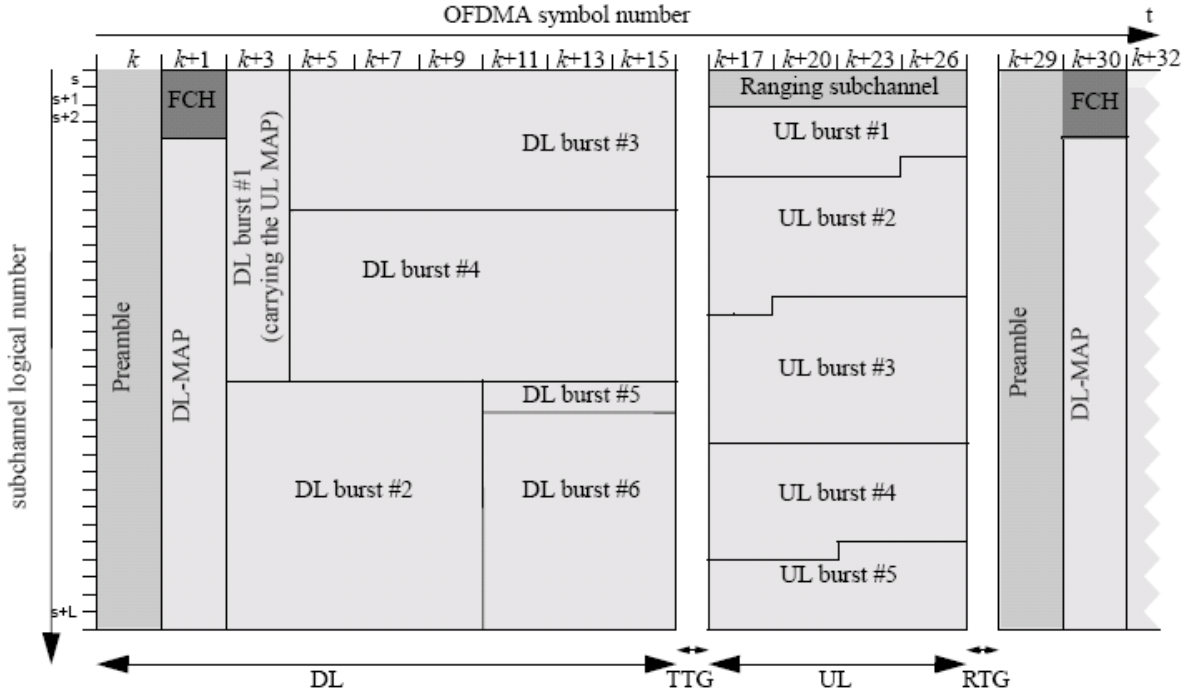

Fig. 3.1 An OFDM frame structure in TDD mode

For supporting various physical channel conditions, IEEE 802.16e defines two modes of sub-channel building method: the distributed subcarrier permutation mode, including partial usage of sub-channels (PUSC) and full usage of sub-channels (FUSC) types, and the adjacent subcarrier permutation mode, including adaptive modulation and coding (AMC) type.

In this thesis, PUSC mode is mainly supported and more details of the subcarrier allocation scheme were described in Section 3.3 of [3].

3.1.2 Preamble Format

The preamble symbol consists of a specific pattern known to the receiver and occupies the duration of an OFDM symbol time. It is used for frame detection, synchronization and initial channel estimation. IEEE 802.16e standard provides three types of carrier set for different

segments in preamble symbol which can be expressed as

$$\Pr eambleCarrierSet_s = s + 3 \cdot k \tag{3.1}$$

where $s \in \{0,1,2\}$ is the index of the subcarrier set, and k denotes a running subcarrier index. These subcarriers in the preamble symbol are modulated by binary phase shift keying (BPSK) with a specific Pseudo-Noise (PN) code. The PN series modulating the pilots in preamble can be found in [1]. Each segment in a zone uses one type of preamble carrier set. For different FFT size, there are total 114 PN series to be chosen by the ID cell parameter and the segment index. The guard band subcarriers are contained both on the left and right side of the spectrum. The DC subcarrier is always be zeroed even if the type of carry set is 0. The power of the preamble subcarrier is boosted by a factor, $2\sqrt{2}$, to increase the reliability of preamble. The pilot subcarrier p_k in the preamble symbol are modulated as

$$\mathrm{Re}\{p_k\} = 4\sqrt{2} \cdot \left(\frac{1}{2} - w_k\right), \quad \mathrm{Im}\{p_k\} = 0 \tag{3.2}$$

where w_k denotes the PN series, and $\mathrm{Re}\{\bullet\}$ and $\mathrm{Im}\{\bullet\}$ stands for the real and imaginary part of $\{\bullet\}$.

3.1.3 Pilot Modulation

The OFDM symbol structure is constructed using pilots, data, and null subcarriers. The symbol is first divided into basic clusters and null carriers are allocated. In down link PUSC mode, pilots and data carriers are allocated within each cluster as shown in Fig. 3.2. For the proposed system with two transmit antennas, when the pilot subcarrier is transmitted from one antenna, the other antenna will not transmit a pilot in the same subcarrier to avoid inter-antenna interference. The pilot location schemes periodically change every four OFDM symbols.

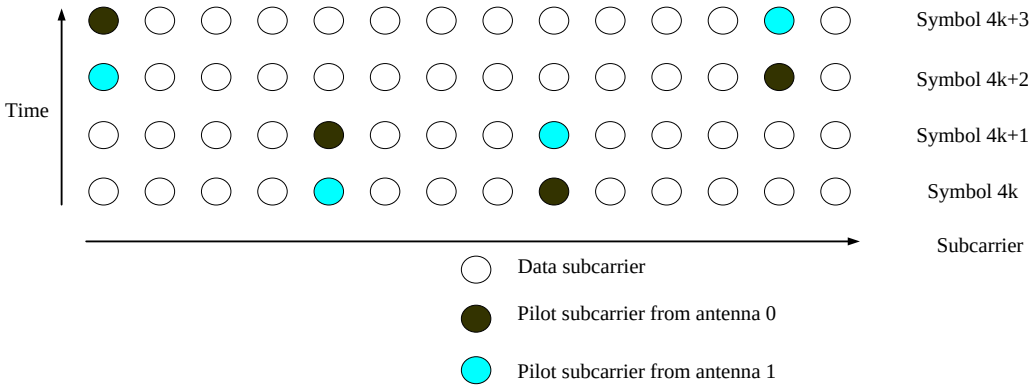

Fig.3.2 Pilot cluster structure

Each pilot is boosted 2.5dB over the average non-boosted power of each data subcarriers. The value of the pilot modulation on subcarrier k shall be derived from a pseudo-random sequence z_k. The pilot subcarriers p_k are modulated as

$$\mathrm{Re}\{p_k\} = \frac{8}{3}\left(\frac{1}{2} - z_k\right), \quad \mathrm{Im}\{p_k\} = 0 \tag{3.3}$$

3.1.4 Differences Between 802.16e and 802.16m

IEEE 802.16m [2] provides continuity to the first released of Mobile WiMAX (802.16e) and offer evolution path to existing WiMAX operators and win new operators targeting the deployments from 2012. It improves system performance, enables more flexible radio network architecture, and is fully backward compatible with 802.16e. The main differences between 802.16m and 802.16e are summarized in Table 3.1.

Table 3.1 802.16e and 802.16m comparison

Feature	IEEE 802.16e	IEEE802.16m
Duplexing Modes	TDD	TDD, FDD
Channel Bandwidths	5, 3.5, 7, 8.75, 10 MHz	5, 10, 20, 40 MHz
Peak Data Rate	DL: 64 Mbps@ 10MHz UL: 28 Mbps@ 10MHz	DL: >300 Mbps@ 20MHz UL: >135 Mbps@ 20MHz
Mobility	Up to 120 km/hr	Up to 350 km/hr
MIMO Configuration	DL: 2x2 UL: 1x2	DL: 2x2, 2x4, 4x2, 4x4 UL: 1x2, 1x4, 2x2, 2x4
Average Sector Throughput TDD (DL:UL=2:1)	DL: 25Mbps UL: 6Mbps @ 10MHz	DL: > 35 Mbps UL:>8.7 Mbps @20MHz
Latency	Link-Layer Access: 20ms Handoff : 35-50ms	Link-Layer Access: <10ms Handoff : <30ms
Coverage	1, 5, 30 km	1, 5, 30 km (optimal at 5km)
Number of VoIP Active Users	~ 25 users/sector/MHz	> 60 users/sector/MHz

3.1.5 Major Parameters and Design Targets

The IEEE 802.16e specification for multi antenna technique is adopted in the proposed STBC-OFDM system, and the major parameters are summarized in Table 3.2.

Table 3.2 Major parameters of proposed STBC-OFDM system

Parameters		**Deriving formulas**	**Values**
FFT size (N)			1024
Symbol Length (N_s)			1152
Cyclic Prefix Length (N_g)			128
System channel bandwidth (BW)			10 MHz
Sampling frequency (F_s)			11.2 MHz
Subcarrier spacing (Δf)		F_s / N	10.94 kHz
Useful symbol time (T_b)		$1/\Delta f$	91.4 us
Guard time (T_g)		$(N_g / N_s) \cdot T_b$	11.4 us
OFDMA symbol duration (T_s)		$T_b + T_g$	102.8 us
Frame duration (T_F)			5 ms
PUSC	Number of null subcarriers (N_n)		184
	Number of clusters (N_u)	$(N_{FFT} - N_n)/14$	60
	Number of pilot subcarriers (N_p)	$N_u \times 2$	120
	Number of data subcarriers (N_d)	$N_u \times 12$	720
Design Target			
Modulation Mode			16QAM
Uncoded Data Rate			27.32 Mbps
Vehicle Speed			Up to 360 km/h
Normalized Maximum Doppler Frequency ($f_d / \Delta f$)			0.075
Improve BER performance with acceptable computational complexity.			

The system occupies a bandwidth of 10 MHz and operates in 2.5GHz frequency band. The sampling frequency is 11.2 MHz. FFT size (N) is set to 1024. Each OFDM symbol is composed of 1024 subcarriers, among which 720 and 120 subcarriers are data and pilots. The remaining 184 subcarriers are used either as a DC subcarrier or virtual subcarriers. In 802.16e, the modulation scheme of QPSK, 16QAM, and 64-QAM are supported for data subcarriers, while only QPSK is adopted for pilot subcarriers and preamble symbol. The length of cyclic prefix (CP) is 128 sampling periods, equivalent to 1/8 of the useful symbol interval (T_b).

Fig. 3.3 depicts the frame format which starts with one preamble and is followed by 40 successive OFDM data symbols. A time slot is equivalent to the time duration of two OFDM symbols.

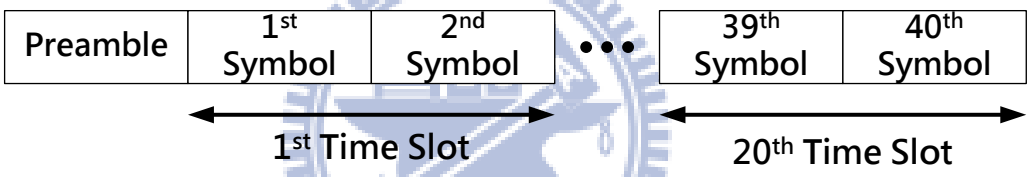

Fig. 3.3 Frame format

Originally, the proposed STBC-OFDM system and channel estimator design [3] is optimized for vehicle speed 120 km/h. In this thesis, we propose an STBC interference canceller to improve system performance and enable vehicle speed up to 360 km/h. The coherence time at this speed is $T_c = 0.423/f_d = 0.75$ ms, which is about 7.4 times of an OFDM symbol period and is smaller than one frame. Theoretically, the channel should be treated as quasi-static. Under the assumption that the channel variation inside one time slot is insignificant, one should intuitively think of ICI as the major interference noise that hampers the accuracy of STBC decoding.

However, it has been shown that even if ICI is perfectly cancelled and the coherence time is as long as 13.3 times of an OFDM symbol, the system performance would be severely corrupted by CCI noise alone [6]. Furthermore, it has been demonstrated that CCI power is

larger than ICI power about 7~8 dB regardless of the channel variation rate [7]. Therefore, with the aid of proposed STBC interference canceller, a significant improve of system performance can be expected, and the design targets are listed in the bottom rows of Table. 3.1.

3.2 Overview of DFT-based Channel Tracking Estimation

STBC-OFDM exploits transmission diversity to provide system performance improvement. However, for STBC decoding and our proposed STBC interference canceller, accurate channel state information (CSI) is essential. It is very difficult to obtain in mobile wireless channels. Therefore, high quality channel estimator with acceptable hardware complexity would be an advantage for our proposed STBC interference canceller. An DFT-based two stage channel estimator has been proposed in [3] to serve our purpose, and we will introduce its principle and architecture in this section.

3.2.1 Two-Stage Channel Tracking Estimation Method

Various DFT-based channel estimation method has been studied using either minimum mean square error (MMSE) criterion or maximum likelihood (ML) criterion have been studied for OFDM system with preambles [10, 11]. Since CSI and signal to noise ratio (SNR) are unavailable at receiver in real implementation, the ML scheme is easier to implement than MMSE scheme. Moreover, the decision-feedback (DF) scheme can be adopted in DFT-based channel estimation to use decision data as pilot to track channel variations for providing sufficient tracking information. Recently, Ku and Huang [12] presented a two-stage DF DFT-based method to apply in STBC-OFDM systems under fast time-varying multipath channels. They concluded that a refined two-stage channel estimator is more robust than classical DFT-based method.

An initialization stage uses a multipath interference cancellation (MPIC)-based decorrelation method to identify the significant paths of channel impulse response (CIR) in the beginning of each frame. However, the CIR estimated by the preamble cannot be directly applied in the following data bursts since the channel is time-variant. Thus a tracking stage is

then used to track the path gains with known CIR positions. The details are described as follows.

(A) Initialization Stage

First, two parameters N_P and $\mathbf{W}_B$ are defined as a presumptive path number of a channel and an observation window set, respectively. Second, the cyclic cross-correlation $C_{\mathrm{RP}}[\tau]$ between the received and transmit preambles as well as the normalized cyclic auto-correlation $C_{\mathrm{PP}}[\tau]$ of the transmitted preambles are calculated. The index l and κ which stand for a path computing variable and the number of legal paths found by the MPIC-based decorrelation are initialized to zero. Third, the process is found by picking only path whose time delay τ_l yields the largest value in $C_{\mathrm{RP}}[\tau]$, for $\tau_l \in \mathbf{W}_B$. If the path delay τ_l is larger than the length of CP, this path is treated as an illegal path and discarded by setting $C_{\mathrm{RP}}[\tau_l]=0$. Otherwise, this path is recorded as the κ-th legal path with a time delay $\tau_\kappa = \tau_l$ and a averaged complex path gain $\bar{\mu}_l = C_{\mathrm{RP}}[\tau_l]$. Note that $\bar{\mu}_l$ is an estimation of the actual averaged complex path gain $\bar{h}_l$ in (2.11).

Then, the interference associated with this legal path is canceled from $C_{\mathrm{RP}}[\tau]$ to obtain a refined cross-correlation function

$$C_{\mathrm{RP}}[\tau] = C_{\mathrm{RP}}[\tau] - \mu_\kappa C_{\mathrm{PP}}[|\tau-\tau_\kappa|], \quad \tau \in \mathbf{W}_B \setminus \{\tau_0,\cdots,\tau_{l-1}\} \tag{3.4}$$

Meanwhile, κ is increased by one. The value of l is also increased by one at the end of each iteration, and the iterative process is continued until l reaches the presumed value of N_P.

(B) Tracking Stage

After initialization stage, we can obtain the information of the path number $\kappa^{(i)}$, the

multipath delays $\tau_l^{(i)}$, the averaged multipath complex gains $\bar{\mu}_l^{(i)}$, for $l \in \{0,\cdots,\kappa^{(i)}-1\}$, and the corresponding CFRs, where i is corresponding to the i-th transmit antenna. Under the assumption that the multipath delays do not change over the duration of a frame, the DF DFT-based channel estimation method in ts-th time slot can be equivalently expressed in Newton's method as [13]

$$\delta_{ts,\nu}[k] = \mathrm{M}_{ts,\nu\text{-}1}[k] - \frac{1}{\left(\left|X_{F,\nu}\right|^2 + \left|X_{S,\nu}\right|^2\right)} \begin{bmatrix} X_{F,\nu} & X_{S,\nu} \\ -X_{S,\nu}^{*} & X_{F,\nu}^{*} \end{bmatrix}^H \begin{bmatrix} R_{ts}[1,k] \\ R_{ts}[2,k] \end{bmatrix} \tag{3.5}$$

$$\begin{aligned} \mathrm{q}_{ts,\nu}^{(i)} &= \mathrm{F}_{\mathrm{IDFT}}^{(i)} \Delta_{ts,\nu}^{(i)} \\ \mathrm{F}_{\mathrm{DFT}}^{(i)}[m,l] &= e^{-j2\frac{m}{N}\tau_l^{(i)}} \quad ; \forall m \in \{0,1,\cdots,N-1\}, l \in \{0,1,\cdots,L-1\} \end{aligned} \tag{3.6}$$

$$\mathrm{M}_{ts,\nu}^{(i)} = \mathrm{M}_{ts,\nu-1}^{(i)} - \mathrm{F}_{\mathrm{DFT}}^{(i)} \left[\mathrm{E}^{(i)}\right]^{-1} \mathrm{q}_{ts,\nu}^{(i)} \tag{3.7}$$

The vector $\delta_{ts,\nu}[k] = \{\Delta_{ts,\nu}^{(i)}[k] : i = 1,2\}$ calculates the difference between the previous estimated CFR vector $\mathrm{M}_{ts,\nu-1} = \{M_{ts,\nu-1}^{(i)} : i = 1,2\}$ and the least-square (LS) estimated CFR of the ts-th time slot, where the subscript ν stands for the iteration index. The inverse DFT (IDFT) matrix $\mathrm{F}_{\mathrm{DFT}}^{(i)}$ multiplying by $\Delta_{ts,\nu}^{(i)}$ in (3.6) is to form the gradient vector $\mathrm{q}_{ts,\nu}^{(i)}$ in Newton's method. In addition, the weighting matrix $\left[\mathrm{E}^{(i)}\right]^{-1}$ in (3.7) is in fact the inverse of the Hessian matrix in Newton's method. The (l,l')-th entry of $\mathrm{E}^{(i)}$ is given by

$$\mathrm{E}^{(i)}[l,l'] = \sum_{k\in\Theta} \cos\left(\frac{2\pi k\left(\tau_l^{(i)} - \tau_{l'}^{(i)}\right)}{N}\right) + j\sum_{k\in\Theta} \sin\left(\frac{2\pi k\left(\tau_l^{(i)} - \tau_{l'}^{(i)}\right)}{N}\right) \tag{3.8}$$

where $\boldsymbol{\Theta}$ is a subset of data subcarrier indices.

In this channel estimation method, pilot symbols as well as data symbols are simultaneously adopted to perform tracking iterations. From the view point of optimization, since pilots inserted in each OFDM symbol are more reliable than the decided data symbols,

they should play a dominant role in providing a global direction search at the first tracking iteration. Thus, the first iteration of the channel tracking is modified as

$$M_{ts,1}^{(i)} = M_{ts,0}^{(i)} - \varphi \cdot F_{DFT}^{(i)} q_{ts,\nu}^{(i)} \tag{3.9}$$

where the gradient vector $q_{\nu}^{(i)}$ is calculated according to (3.5)-(3.6) by using the pilot subcarrier set $\mathbf{J}$ instead of the set $\mathbf{\Theta}$, and the value φ is an experimental constant of step size to provide the best performance.

3.2.2 Channel Estimator Architecture

Based on the two stage DFT based algorithm studied in [12], an low complexity and accurate implementation was proposed by [3]. The overall block diagram of this proposed channel estimator is shown in Fig.3.4. The initialization stage is decomposed to a preamble match, an IFFT, a straight MPIC (SMPIC)-based decorrelator, and an FFT. The tracking stage is decomposed to a STBC decoder, a demapper, an LS estimator, an IFFT, a path decorrelator, a Hessian matrix calculator, and an IFFT. Moreover, the IFFT and FFT are shared between the initialization stage and the tracking stage.

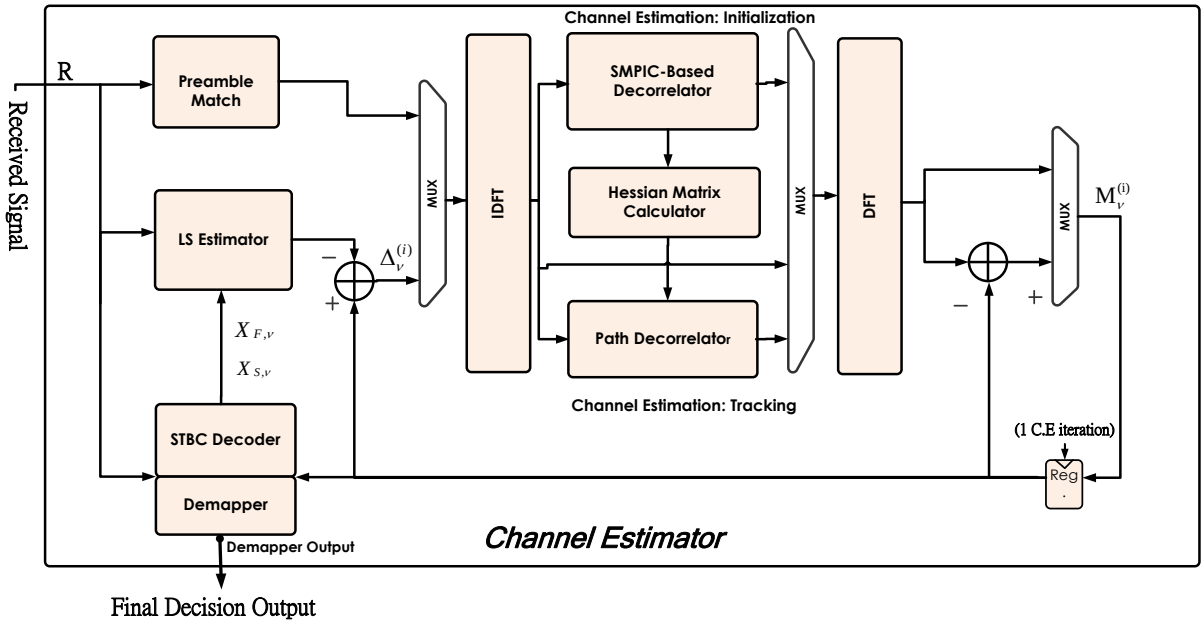

Fig. 3.4 Overall block diagram of the implemented channel estimator

3.3 Co-carrier Interference modeling

CCI noise component in STBC-OFDM system was defined by (2.20). It results from channel variation between two symbol intervals inside one time slot. Various studies has demonstrated that CCI is the major impact on STBC-OFDM system [6-9], so CCI problem shall be solved first than ICI problem in our proposed algorithm.

To calculate CCI noise, we need to know the frequency domain channel matrix of two OFDM symbol intervals between two transmit antennas and receive antenna, i.e., $\mathrm{H}_{ts,b}^{(i)}[k,k],\ b \in \{1,2\}, i \in \{1,2\}, k \in \{0,1,\cdots,N-1\}$. Nevertheless, most channel estimator design for STBC-OFDM system are aimed at estimating the averaged CFR over two symbol intervals inside one time slot, not the CFR of each symbol interval. The goal of this thesis is to provide an efficient solution for any existing STBC-OFDM systems suffering interference, so we propose an algorithm using only the existing time slot CFR estimation results to approximate the CFR of the two symbol intervals inside the time slot.

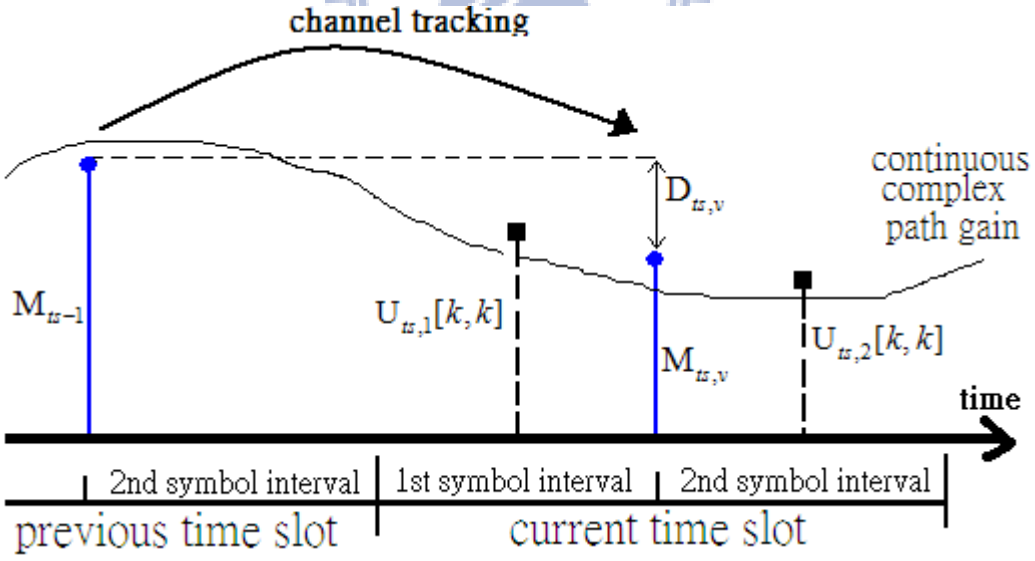

Fig.3.5 Relationship between CFR estimations in time domain

Fig.3.5 demonstrates the relationship between CFR tracking estimations in time domain, where $\mathrm{M}_{ts,v}$ denotes the estimated CFR of the v-th tracking iteration in current time slot,

M_{ts-1} denotes the final CFR estimation of previous time slot, and $\mathrm{D}_{ts,v} = \mathrm{M}_{ts-1} - \mathrm{M}_{ts,v}$. $\mathrm{U}_{ts,1}[k,k]$, $\mathrm{U}_{ts,2}[k,k]$ represents our approximated CFR of the 1st and 2nd symbol interval respectively, and $k \in \{0,1,\cdots,N-1\}$. We should note that no matter what method is used to obtain $\mathrm{U}_{ts,1}[k,k]$ and $\mathrm{U}_{ts,2}[k,k]$, the following constraint shall hold

$$\frac{1}{2}\left(\mathrm{U}_{ts,1}[k,k] + \mathrm{U}_{ts,2}[k,k]\right) = \mathrm{M}_{ts,v} \tag{3.10}$$

A low cost solution for $\mathrm{U}_{ts,1}[k,k]$ is to interpolate the already existed information, $\mathrm{M}_{ts,v}$ and M_{ts-1}. But the estimation of CFR in the 2nd symbol interval, $\mathrm{U}_{ts,2}[k,k]$, is not-causal for real implementation, a predictive approach is needed.

In the study of [14], three types of predictive model are proposed for time varying channel using only previous information from estimator. First one, the zeroth order predictive model assume the variation between $\mathrm{U}_{ts,2}[k,k]$ and $\mathrm{M}_{ts,v}$ can be ignored, and simply set them equal, $\mathrm{U}_{ts,2}[k,k] = \mathrm{M}_{ts,v}$. The second one is the 1st order predictive model; it assumes the variation of CFRs separated by the same time interval are the same. In other word, $\mathrm{U}_{ts,2}[k,k]$ is linearly extrapolated from $\mathrm{M}_{ts,v}$ and M_{ts-1}. The last one is the 2rd order predictive model; it extrapolates $\mathrm{U}_{ts,2}[k,k]$ using 2nd order fitting, and requires the CFR estimation of the previous two time slots. They concluded that the 1st order predictive model outperforms the other two under time varying channel. Moreover, only by applying the 1st order predictive model on $\mathrm{U}_{ts,2}[k,k]$, we can interpolate $\mathrm{U}_{ts,1}[k,k]$ independently without violating the constraint in (3.10). As a result, our proposed approximation is given by

$$\begin{aligned} \mathrm{U}_{ts,1}[k,k] &= \frac{3}{4}\mathrm{M}_{ts,v} + \frac{1}{4}\mathrm{M}_{ts-1} \quad \text{, (linear interpolation)} \\ \mathrm{U}_{ts,2}[k,k] &= \frac{5}{4}\mathrm{M}_{ts,v} - \frac{1}{4}\mathrm{M}_{ts-1} \quad \text{,(linear extrapolation)} \end{aligned} \tag{3.11}$$

3.4 Inter-carrier Interference modeling

In time variant channel, both CCI and ICI appears in STBC-OFDM systems, and CCI component has been proved to be more significant than ICI component. As a result, proposed schemes for STBC interference cancellation target only on CCI and simply ignore ICI problem[6-9]. In this section, we will propose a low complexity algorithm to model ICI by exploiting the information used for CCI modeling in section 3.3. In this way, CCI and ICI noise can be cancelled simultaneously with little overhead. The variant ICI noise γ_{ts} is comparably smaller than β_{ts}, and it's very difficult to obtain an accurate estimation from existing time slot CFR. So we ignore this component and focus on modeling the averaged ICI noise.

3.4.1 Polynomial Modeling of Channel Variation

The averaged frequency domain matrix $\overline{\mathbf{H}}_{ts}^{(i)}$ is defined in (2.11) and (2.18). It requires temporal variation complex gain inside each useful symbol interval but the channel estimator provides only the temporal averaged CSI. As a result, we adopt a LS fitted polynomial method [15-20] to model the detail of the l-th complex path gains between the i-th transmit antennas and receive antenna, as follows:

$$\mu_l^{(i)}[q] = \sum_{d=0}^{N_c-1} \kappa^{(i)}[l,d] q^d + \varepsilon_l[q] \tag{3.12}$$

where $\mu_l^{(i)}[q]$ is the modeled complex path gain at time sample q, $\kappa^{(i)}[l,d]$ is the d-th order complex polynomial coefficient, $d \in \{0,1,\cdots,N_c-1\}$, and (N_c-1) denotes the order of the LS fitting polynomial. It requires N_c observations to solve this (N_c-1)-th order LS fitting problem, so we consider the estimated CFR of the latest N_c time slots and group them as a observation block for each ICI modeling computation. As illustrated in Fig.3.6, every time slot inside an observation block is distinguished by an index, n, where $n = N_c - 1$ stands for the current time slot while $n = 0$ represents the oldest.

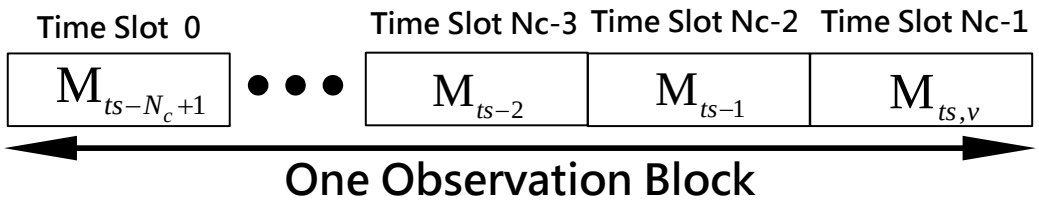

Fig.3.6 The diagram of an observation block

Then, combine (3.12) with the frequency domain channel matrix (2.11), we have

$$\begin{aligned}\overline{\mathrm{U}}_{ts}^{(i)}[k,m] &= \frac{1}{2}\sum_{b=1}^{2}\mathrm{U}_{ts,b}^{(i)}[k,m] \\ &= \frac{1}{2N}\sum_{l=1}^{L}\left\{\sum_{q=0}^{N-1}\left\{\sum_{b=0}^{1}\sum_{d=0}^{N_c-1}\left(\kappa^{(i)}[l,d]\cdot\left(N_g+\left(2\left(N_c-1\right)+b\right)N_s+q\right)^d\right)e^{j2\pi\frac{m-k}{N}q}\right\}e^{-j2\frac{m}{N}\tau_l^{(i)}}\right\} \\ &= \sum_{d=0}^{N_c-1}\mathrm{Q}^{(i)}[m,d]\cdot\Psi_{N_c,d}[k,m] \quad , \forall k,m\in\{0,1,2,\cdots,N-1\}\end{aligned} \tag{3.13}$$

where $\mathrm{U}_{ts,b}^{(i)}$ denotes the estimated channel matrix $\mathrm{H}_{ts,b}^{(i)}$, $\overline{\mathrm{U}}_{ts}^{(i)}$ denotes the estimator of $\overline{\mathrm{H}}_{ts}^{(i)}$, and the two parts decomposed from $\overline{\mathrm{U}}_{ts}^{(i)}$ can be given by

$$\begin{aligned}\mathrm{Q}^{(i)}[m,d] &\triangleq \sum_{l=1}^{L}\kappa^{(i)}[l,d]\cdot e^{-j2\frac{m}{N}\tau_l^{(i)}} = \sum_{l=1}^{L}\mathrm{F}_{\mathrm{DFT}}^{(i)}[m,l]\cdot\kappa^{(i)}[l,d] \\ \Psi_{n,d}[k,m] &\triangleq \frac{1}{2N}\sum_{q=0}^{N-1}\left\{\left(\sum_{b=0}^{1}\left(N_g+\left(2n+b\right)N_s+q\right)^d\right)e^{j2\pi\frac{m-k}{N}q}\right\}\end{aligned} \tag{3.14}$$

$\mathrm{Q}^{(i)}[m,d]$ defines the new polynomial coefficient in frequency domain, and $\Psi_{n,d}[k,m]$ is a fixed value that can be precomputed.

If we define the following identity

$$\Phi_0[k,m] \triangleq \frac{1}{N}\sum_{q=0}^{N-1} e^{j2\pi\frac{m-k}{N}q} = \begin{cases} 1 \text{ , if } k=m \\ 0 \text{ , otherwise} \end{cases}$$

$$\Phi_1[k,m] \triangleq \begin{cases} \dfrac{N-1}{2} \text{ , if } k=m \\ \dfrac{1}{N}\sum_{q=0}^{N-1} q\cdot e^{j2\frac{m-k}{N}q} \text{ , otherwise} \end{cases} \tag{3.15}$$

$$\Phi_2[k,m] \triangleq \begin{cases} \dfrac{(N-1)(2N-1)}{6} \text{ , if } k=m \\ \dfrac{1}{N}\sum_{q=0}^{N-1} q^2\cdot e^{j2\frac{m-k}{N}q} \text{ , otherwise} \end{cases}$$

, then $\Psi_{n,d}[k,m]$ can be simplified as

$$\begin{aligned} \Psi_{n,0}[k,m] &= \Phi_0[k,m] \\ \Psi_{n,1}[k,m] &= \Phi_1[k,m] + \frac{(2z+N_s)}{2}\Phi_0[k,m] \\ \Psi_{n,2}[k,m] &= \Phi_2[k,m] + (2z+N_s)\cdot\Phi_1[k,m] + \frac{2z^2+2z\cdot N_s+N_s^{\,2}}{2}\cdot\Phi_0[k,m] \\ z &= N_g + 2n\cdot N_s \end{aligned} \tag{3.16}$$

On the other hand, if we define

$$\mathrm{T}[r,s] \triangleq \frac{1}{2N}\left(\sum_{q=(2s)\cdot N_s+N_g}^{(2s+1)\cdot N_s-1} q^{(r)} + \sum_{q=(2s+1)\cdot N_s+N_g}^{(2s+2)\cdot N_s-1} q^{(r)} \right) ;\ \forall r,s \in \{0,1,\cdots,N_c-1\} \tag{3.17}$$

, we can obtain the frequency domain polynomial coefficients from CFR estimations inside observation block through the following matrix multiplication:

$$\begin{aligned} \mathrm{Q}^{(i)} &= \mathrm{P}^{(i)}\cdot\mathrm{T}^{-1} \\ \mathrm{P}^{(i)} &= \begin{bmatrix} \mathrm{M}^{(i)}_{ts-N_c+1} & \cdots & \mathrm{M}^{(i)}_{ts-1} & \mathrm{M}^{(i)}_{ts,v} \end{bmatrix} \end{aligned} \tag{3.18}$$

where $\mathrm{P}^{(i)}$ stands for an N -by- N_c matrix formed by using the estimated CFRs as its column vectors.

3.4.2 Simplified Frequency Domain Channel Matrix

Equation (3.13) can be reformulated into matrix form as

$$\overline{\mathrm{U}}_{ts}^{(i)} \triangleq \sum_{d=0}^{N_c-1} diag\left\{\mathrm{Q}^{(i)}[:,d]\right\} \cdot \Psi_{n,d} \tag{3.19}$$

where $diag\{V\}$ denotes a diagonal matrix with vector V on its main diagonal, $\mathrm{Q}^{(i)}[:,d]$ stands for the $\boldsymbol{d-th}$ column vector of $\mathrm{Q}^{(i)}$. According to (3.19), our estimated frequency channel matrix is composed of constant matrix $\Psi_{n,d}$ which models the shape of Doppler spread and the variable part $diag\left\{\mathrm{Q}^{(i)}[:,d]\right\}$ which is linearly transformed from the observed CFRs. We can further simplify our estimator by defining the following linear transformation matrices E_n given by

$$\mathrm{E}=\begin{cases} \mathrm{T}^{-1}\cdot\begin{bmatrix} 1 & 0 & 0 \\ \dfrac{2c+N_s}{2} & 1 & 0 \\ \dfrac{2c^2+2c\cdot N_s+N_s^2}{2} & 2c+N_s & 1 \end{bmatrix} & ;\text{if } N_c=3 \\ \mathrm{T}^{-1}\cdot\begin{bmatrix} 1 & 0 \\ \dfrac{2c+N_s}{2} & 1 \end{bmatrix} & ;\text{if } N_c=2 \end{cases} \tag{3.20}$$

$$c = N_g + 2\left(N_c-1\right)\cdot N_s$$

In this way, all linear operations can be precomputed outside of the diagonal matrix, which gives

$$
\begin{aligned}
&\text{For } N_c = 2: \\
&\quad \overline{\mathrm{U}}_{ts}^{(i)} = diag\left\{\mathrm{M}_{ts-1}^{(i)}\right\}\cdot\left(\mathrm{E}[0,0]\cdot\Phi_0 + \mathrm{E}[0,1]\cdot\Phi_1\right) + diag\left\{\mathrm{M}_{ts,v}^{(i)}\right\}\cdot\left(\mathrm{E}[1,0]\cdot\Phi_0 + \mathrm{E}[1,1]\cdot\Phi_1\right) \\
&\text{For } N_c = 3: \\
&\quad \overline{\mathrm{U}}_{ts}^{(i)} = diag\left\{\mathrm{M}_{ts-2}^{(i)}\right\}\cdot\left(\mathrm{E}[0,0]\cdot\Phi_0 + \mathrm{E}[0,1]\cdot\Phi_1 + \mathrm{E}[0,2]\cdot\Phi_2\right) \\
&\qquad + diag\left\{\mathrm{M}_{ts-1}^{(i)}\right\}\cdot\left(\mathrm{E}[1,0]\cdot\Phi_0 + \mathrm{E}[1,1]\cdot\Phi_1 + \mathrm{E}[1,2]\cdot\Phi_2\right) \\
&\qquad + diag\left\{\mathrm{M}_{ts,v}^{(i)}\right\}\cdot\left(\mathrm{E}[2,0]\cdot\Phi_0 + \mathrm{E}[2,1]\cdot\Phi_1 + \mathrm{E}[2,2]\cdot\Phi_2\right)
\end{aligned}
\tag{3.21}
$$

By observing (3.20), we can realize the following identities

$$
\begin{aligned}
&\text{For } N_c = 2: \\
&\qquad \mathrm{E}[0,0] + \mathrm{E}[1,0] = 0 \\
&\text{For } N_c = 3: \\
&\qquad \mathrm{E}[0,0] + \mathrm{E}[1,0] + \mathrm{E}[2,0] = 0 \\
&\qquad \mathrm{E}[0,1] + \mathrm{E}[1,1] + \mathrm{E}[2,1] = 0
\end{aligned}
\tag{3.22}
$$

, thereby final expression of averaged frequency channel matrix estimation is given by

$$
\begin{aligned}
&\text{For } N_c = 2: \\
&\quad \overline{\mathrm{U}}_{ts}^{(i)}[k,m] = \begin{cases} \left(\mathrm{M}_{ts-1}^{(i)}[k] - \mathrm{M}_{ts,v}^{(i)}[k]\right)\cdot \mathrm{G}_0[k,m] & ;\ \text{if } k \neq m \\ \mathrm{M}_{ts,v}^{(i)}[k] & ;\ \text{if } k = m \end{cases} \\
&\quad \mathrm{G}_0[k,m] \triangleq \begin{cases} \mathrm{E}[0,1]\cdot\Phi_1[k,m] & ;\ \text{if } k \neq m \\ 0 & ;\ \text{if } k = m \end{cases} \\
&\text{For } N_c = 3: \\
&\quad \overline{\mathrm{U}}_{ts}^{(i)}[k,m] = \begin{cases} \left(\mathrm{M}_{ts-2}^{(i)}[k] - \mathrm{M}_{ts-1}^{(i)}[k]\right)\cdot \mathrm{G}_{-1}[k,m] + \left(\mathrm{M}_{ts-1}^{(i)}[k] - \mathrm{M}_{ts,v}^{(i)}[k]\right)\cdot \mathrm{G}_0[k,m] & ;\ \text{if } k \neq m \\ \mathrm{M}_{ts,v}^{(i)}[k] & ;\ \text{if } k = m \end{cases} \\
&\quad \mathrm{G}_{-1}[k,m] \triangleq \begin{cases} \mathrm{E}[0,1]\cdot\Phi_1[k,m] + \mathrm{E}[0,2]\cdot\Phi_2[k,m] & ;\ \text{if } k \neq m \\ 0 & ;\ \text{if } k = m \end{cases} \\
&\quad \mathrm{G}_0[k,m] \triangleq \begin{cases} -\mathrm{E}[2,1]\cdot\Phi_1[k,m] - \mathrm{E}[2,2]\cdot\Phi_2[k,m] & ;\ \text{if } k \neq m \\ 0 & ;\ \text{if } k = m \end{cases}
\end{aligned}
\tag{3.23}
$$

3.4.3 Pilot ICI Component

The modulation of pilot symbols was described in Section 3.1.3. Pilots do not go through STBC encoding before transmission, and the received pilot signals are given by

$$\zeta_{ts}[k]=\sum_{g=0}^{\frac{N_J}{2}}\begin{bmatrix} \mathrm{H}_{ts,1}^{(1)}\left[k,J_{2g+1}\right]+\mathrm{H}_{ts,1}^{(2)}\left[k,J_{2g}\right] & 0 \\ 0 & \left\{\mathrm{H}_{ts,2}^{(1)}\left[k,J_{2g}\right]+\mathrm{H}_{ts,2}^{(2)}\left[k,J_{2g+1}\right]\right\}^{*} \end{bmatrix}\mathrm{P}[g] \quad (3.24)$$

where $\mathrm{P}[\mathrm{g}]$ denotes the pilot symbol of cluster g, $\mathbf{J}=\left\{J_0,J_1,\cdots,J_{N_J-1}\right\}$ represents the pilot subcarrier index set, and N_J denotes the number of elements inside pilot index set $\mathbf{J}$. As in the assumption of data ICI estimation, we assume the variant part of pilot ICI is trivial enough to be ignored, and our pilot ICI estimator is given by

$$\hat{\zeta}_{ts}[k]=\sum_{g=0}^{\frac{N_J}{2}-1}\begin{bmatrix} P[g]\left\{\overline{\mathrm{U}}_{ts}^{(1)}\left[k,J_{2g+1}\right]+\overline{\mathrm{U}}_{ts}^{(2)}\left[k,J_{2g}\right]\right\} \\ \left(P[g]\right)^{*}\left\{\overline{\mathrm{U}}_{ts}^{(1)}\left[k,J_{2g}\right]+\overline{\mathrm{U}}_{ts}^{(2)}\left[k,J_{2g+1}\right]\right\}^{*} \end{bmatrix} \quad (3.25)$$

3.5 Joined Interference Cancellation Algorithm

According to the approximation models derived in Section 3.4, we can derive estimator for each STBC interference noise defined in (2.19). First, the estimation of CCI noise is given by

$$\begin{aligned}\alpha_{ts,\nu}^{(\lambda)}[k] &\triangleq \begin{bmatrix} \left(\overline{\mathrm{U}}_{ts,1}^{(1)}[k,k]-\mathrm{M}_{ts,\nu}^{(1)}[k]\right) & \left(\overline{\mathrm{U}}_{ts,1}^{(1)}[k,k]-\mathrm{M}_{t}^{(2)}[k]\right) \\ \left(\overline{\mathrm{U}}_{t,2}^{(2)}[k,k]-\mathrm{M}_{t}^{(2)}[k]\right)^{*} & -\left(\overline{\mathrm{U}}_{t,2}^{(1)}[k,k]-\mathrm{M}_{ts,\nu}^{(1)}[k]\right)^{*} \end{bmatrix} \mathrm{X}_{\nu}^{(\lambda)}[k] \\ &= \frac{1}{4}\begin{bmatrix} \mathrm{D}_{ts,\nu}^{(1)}[k]X_{F,\nu}^{(\lambda)}[k]+\mathrm{D}_{ts,\nu}^{(2)}[k]X_{S,\nu}^{(\lambda)}[k] \\ -\left(\mathrm{D}_{ts,\nu}^{(2)}[k]\right)^{*}X_{F,\nu}^{(\lambda)}[k]+\left(\mathrm{D}_{ts,\nu}^{(1)}[k]\right)^{*}X_{S,\nu}^{(\lambda)}[k] \end{bmatrix} \\ \mathrm{D}_{ts,\nu}^{(i)} &= \mathrm{M}_{ts-1}^{(i)}-\mathrm{M}_{ts,\nu}^{(i)}\end{aligned} \tag{3.26}$$

where λ denotes the decode iteration index defined in Section 2.4, ν denotes the channel tracking iteration index defined in Section 3.2. Second, the estimation of averaged ICI noise is given by

$$\beta_{ts,\nu}^{(\lambda)}[k] \triangleq \sum_{\substack{m \\ m\in\boldsymbol{\Theta}\setminus k}} \begin{bmatrix} \overline{\mathrm{U}}_{ts}^{(1)}[k,m] & \overline{\mathrm{U}}_{ts}^{(2)}[k,m] \\ \left(\overline{\mathrm{U}}_{ts}^{(2)}[k,m]\right)^{*} & -\left(\overline{\mathrm{U}}_{ts}^{(1)}[k,m]\right)^{*} \end{bmatrix} \mathrm{X}_{\nu}^{(\lambda)}[m] \tag{3.27}$$

In the special case of $N_c = 2$, we can reformulate $\beta_{ts,\nu}^{(\lambda)}[k]$ into a format very similar to (3.26):

$$\beta_{ts,\nu}^{(\lambda)}[k] = \sum_{\substack{m \\ m\in\boldsymbol{\Theta}\setminus k}} \begin{bmatrix} \left(\mathrm{D}_{ts,\nu}^{(1)}[m]X_{F,\nu}^{(\lambda)}[m]+\mathrm{D}_{ts,\nu}^{(2)}[m]X_{S,\nu}^{(\lambda)}[m]\right)\cdot G_0[k,m] \\ \left(\left(\mathrm{D}_{ts,\nu}^{(2)}[m]\right)^{*}X_{F,\nu}^{(\lambda)}[m]-\left(\mathrm{D}_{ts,\nu}^{(1)}[m]\right)^{*}X_{S,\nu}^{(\lambda)}[m]\right)\left(G_0[k,m]\right)^{*} \end{bmatrix} \tag{3.28}$$

Also, it can be observed that $G_0[k,m]$ depends only on the value $|k-m|$, if we define

$$S_b\left[\left|k-m\right|\right]=\begin{cases} G_0\left[k,m\right] \text{ ; if } k\neq m \\ 0.25 \quad \text{; if } k=m,\ b=1 \\ -0.25 \text{ ; if } k=m,\ b=2 \end{cases} \tag{3.29}$$

then (3.26) and (3.28) can be combined together as

$$\alpha_{ts,\nu}^{(\lambda)}\left[k\right]+\beta_{ts,\nu}^{(\lambda)}\left[k\right]=\sum_{\substack{m \\ m\in\mathbf{\Theta}}}\begin{bmatrix} \left(\mathrm{D}_{ts,\nu}^{(1)}\left[m\right]X_{F,\nu}^{(\lambda)}\left[m\right]+\mathrm{D}_{ts,\nu}^{(2)}\left[m\right]X_{S,\nu}^{(\lambda)}\left[m\right]\right)\cdot S_1\left[\left|k-m\right|\right] \\ \left(\left(\mathrm{D}_{ts,\nu}^{(2)}\left[m\right]\right)^{*}X_{F,\nu}^{(\lambda)}\left[m\right]-\left(\mathrm{D}_{ts,\nu}^{(1)}\left[m\right]\right)^{*}X_{S,\nu}^{(\lambda)}\left[m\right]\right)\left(S_2\left[\left|k-m\right|\right]\right)^{*} \end{bmatrix} \tag{3.30}$$

where $S_b\left[0\right]$ models CCI component, and the rest modes the ICI components. We use the result in [4] that when ICI is due to only a few nearest neighboring subcarriers (2W) when the normalized maximum Doppler frequency is small (less than 0.1), and (3.30) becomes

$$\alpha_{ts,\nu}^{(\lambda)}\left[k\right]+\beta_{ts,\nu}^{(\lambda)}\left[k\right]\simeq\sum_{w=-W}^{W}\begin{bmatrix} \left(\mathrm{D}_{ts,\nu}^{(1)}\left[m\right]X_{F,\nu}^{(\lambda)}\left[m\right]+\mathrm{D}_{ts,\nu}^{(2)}\left[m\right]X_{S,\nu}^{(\lambda)}\left[m\right]\right)\cdot S_1\left[\left|w\right|\right] \\ \left(\left(\mathrm{D}_{ts,\nu}^{(2)}\left[m\right]\right)^{*}X_{F,\nu}^{(\lambda)}\left[m\right]-\left(\mathrm{D}_{ts,\nu}^{(1)}\left[m\right]\right)^{*}X_{S,\nu}^{(\lambda)}\left[m\right]\right)\left(S_2\left[\left|w\right|\right]\right)^{*} \end{bmatrix}$$
$$m=\left(k+w\right)_N\in\mathbf{\Theta} \tag{3.31}$$

where $\left(\bullet\right)_N$ denotes modulo-N operation. Similarly, $\hat{\zeta}_{ts}$ can be reformulated as follows:

$$\hat{\zeta}_{ts} \simeq \sum_{\substack{u=-W \\ (k+u)_N = J_{2g} \\ 0 \le g \le \frac{N_J}{2}}}^{W} \left[\left(D_{ts,\nu}^{(2)}\left[(k+u)_N\right] \cdot P\left[\left\lfloor (k+u)_N / 2 \right\rfloor\right] \right) \cdot S_1\left[|u|\right] \right] \left\{ \left(D_{ts,\nu}^{(1)}\left[(k+u)_N\right] \cdot P\left[\left\lfloor (k+u)_N / 2 \right\rfloor\right] \right) \cdot S_2\left[|u|\right] \right\}^* + \sum_{\substack{c=-W \\ (k+c)_N = J_{2g+1} \\ 0 \le g \le \frac{N_J}{2}}}^{W} \left[\left(D_{ts,\nu}^{(1)}\left[(k+c)_N\right] \cdot P\left[\left\lfloor (k+c)_N / 2 \right\rfloor\right] \right) \cdot S_1\left[|c|\right] \right] \left\{ \left(D_{ts,\nu}^{(2)}\left[(k+c)_N\right] \cdot P\left[\left\lfloor (k+c)_N / 2 \right\rfloor\right] \right) \cdot S_2\left[|c|\right] \right\}^* \quad (3.32)$$

where the first and second summation part represents pilot ICI noise from the subcarriers belong to the even and odd pilot index set, respectively.

Finally, by choosing 1st order LS fitting model, the interference noise can be estimated simultaneously using only the latest CFR variation and a set of fixed constant gain S_b. In this way, our proposed algorithm helps save a lot of computational complexity as well as keeps the storage size need for observation block as small as possible.

3.6 Simulation Results

3.6.1 Proposed Algorithm with Perfect Channel Estimation

The following simulations uses perfectly estimated CFR at the receiver, and the STBC decoding flow is defined in Section 2.4. The multipath channel adopt the ITU Veh-A channel model with relative path power profiles of 0, -1, -9, -10, -15, and -20 (dB), and the path excess delays are uniformly distributed from 0 to 50 sampling periods. Jakes model is also used to generate Raleigh fading environment.

Fig.3.7 and Fig.3.8 show the BER performance of the proposed algorithm with different decoding iterations for QPSK and 16QAM modulations at the vehicle speed of 240 km/hr and 360 km/hr. In order to focus on the effect of STBC interference, we set $E_b / N_o = 30$ to ignore AWGN without losing generality. ICI from ten nearest subcarriers (W=5) are considered. The maximum Doppler f_d is 555.6 Hz and the normalized Doppler is 0.05 for vehicle speed 240 km/hr, similarly $f_d = 833.4\,\text{Hz}$ and $f_d / \Delta f = 0.075$ for vehicle speed 360 km/hr. Note that in the case decoding iteration number equals zero, we don't apply interference cancellation and the result is pure Alamouti simple decoding with perfect channel estimation. The results of perfect channel estimation with perfect ICI model, denoted as "Perfect CSI % Proposed Algorithm (Perfect ICI model)", uses (2.11) and is included for benchmarking. As shown in Fig.3.7, our proposed algorithm provides two times improvement for vehicle speed 360 km/hr and one order BER drop for vehicle speed 240 km/hr. The improvements get into saturate at the second decoding iteration. The third order ICI model refers the CFR from previous two time slots, which are unreliable to estimate present channel variation in time-varying environment. Therefore, the third order ICI model doesn't outperform the second model for vehicle speed 240 km/hr and is even worse than second order ICI model for higher speed. The distinct performance gap between perfect ICI model and proposed ICI model is caused by modeling error during simplification. Fig.3.8 presents the case of QPSK modulation. The improvement is less significant than 16QAM modulation, but the three kinds of model have very similar performance. This is because the QPSK modulation itself is robust enough to withstand STBC interference noise; the performances reach the limitation for simple Alamouti decoding

method.

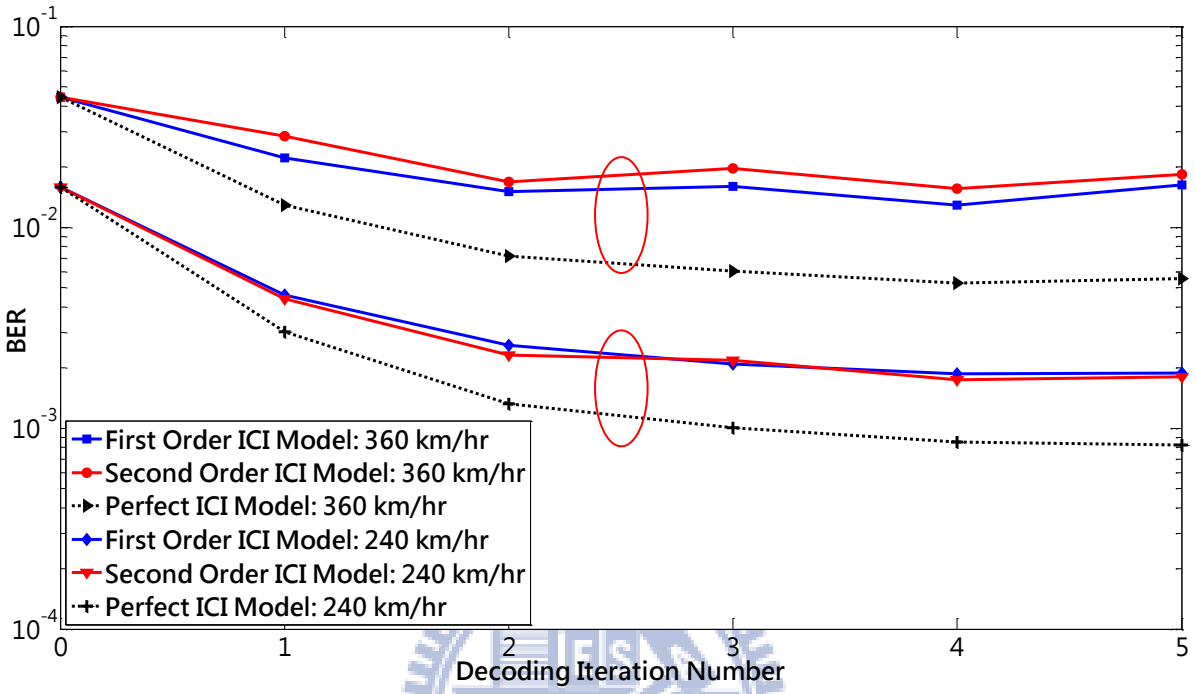

Fig.3.7 BER performances versus decoding iteration number for 16QAM at vehicle speed 360 km/h and 240 km/hr

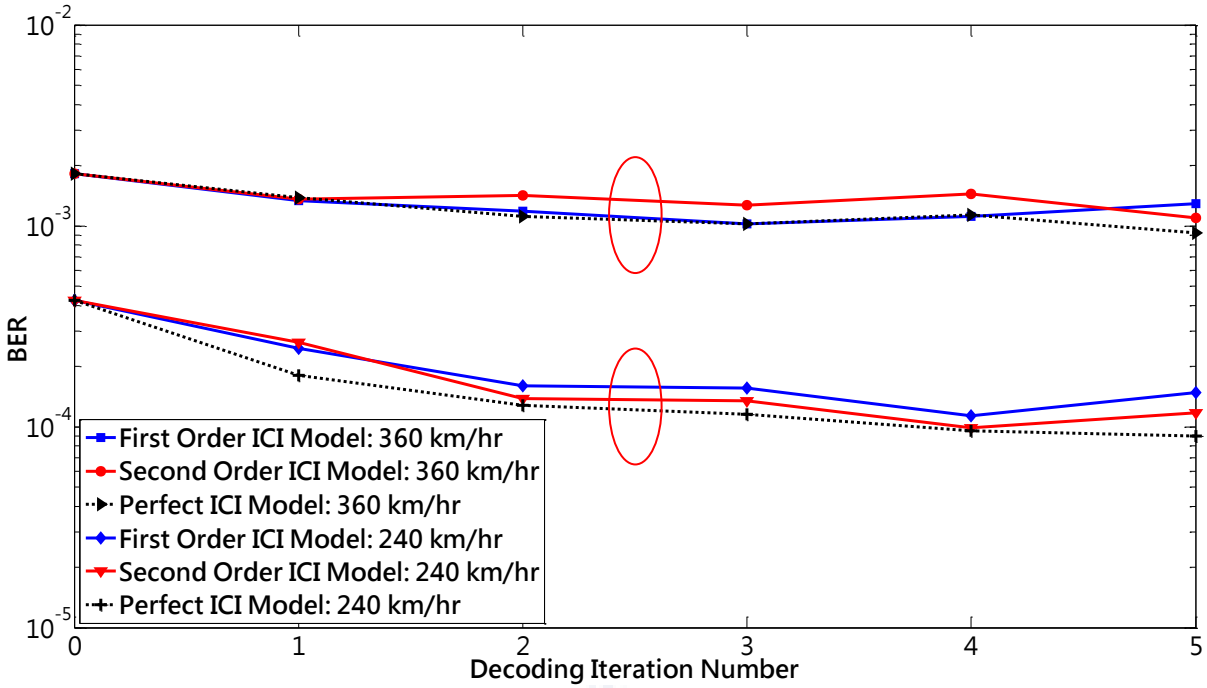

Fig.3.8 BER performances versus decoding iteration number for QPSK at vehicle speed 360 km/h and 240 km/hr

Fig.3.9 and Fig.3.10 shows the BER performance of the proposed algorithm with different range of nearest ICI subcarriers. The variable W of x-axis denotes the range of nearest subcarriers that induce ICI noise, for example, W=5 represents the nearest ten subcarriers are considered. In the case of W=0, all ICI noises are ignored and only CCI cancellation is applied.

From the simulation results, we can conclude that ICI effect at QPSK is very small.

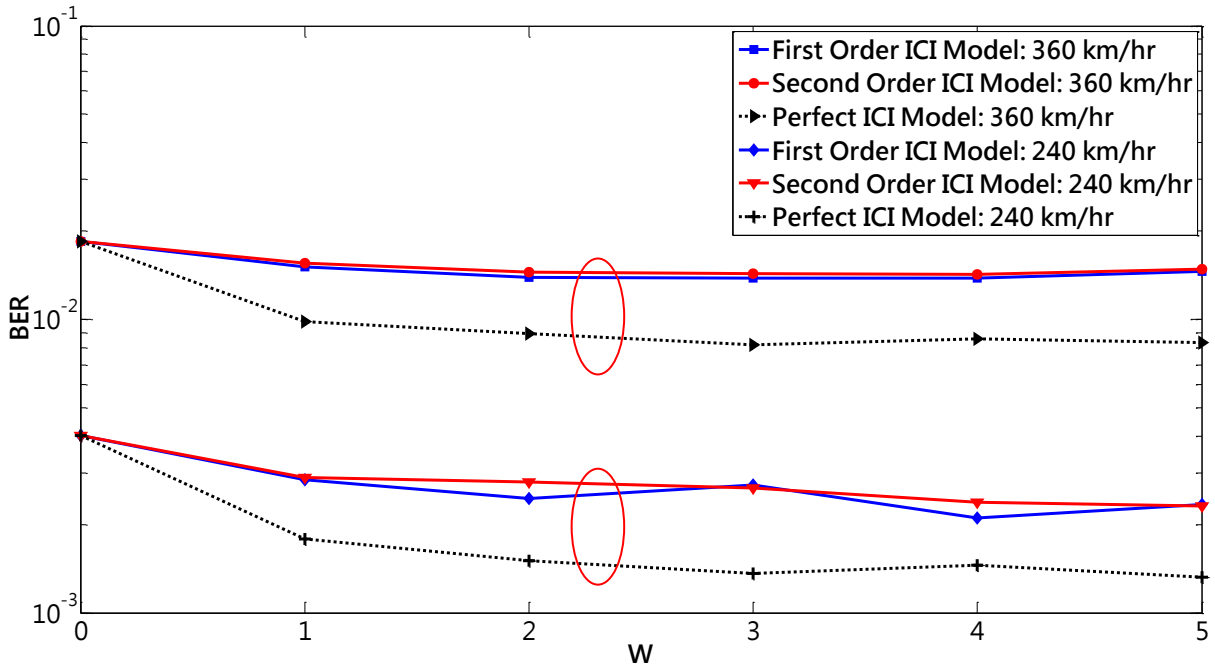

Fig.3.9 BER performances versus decoding iteration number for 16QAM at vehicle speed 360 km/h and 240 km/hr

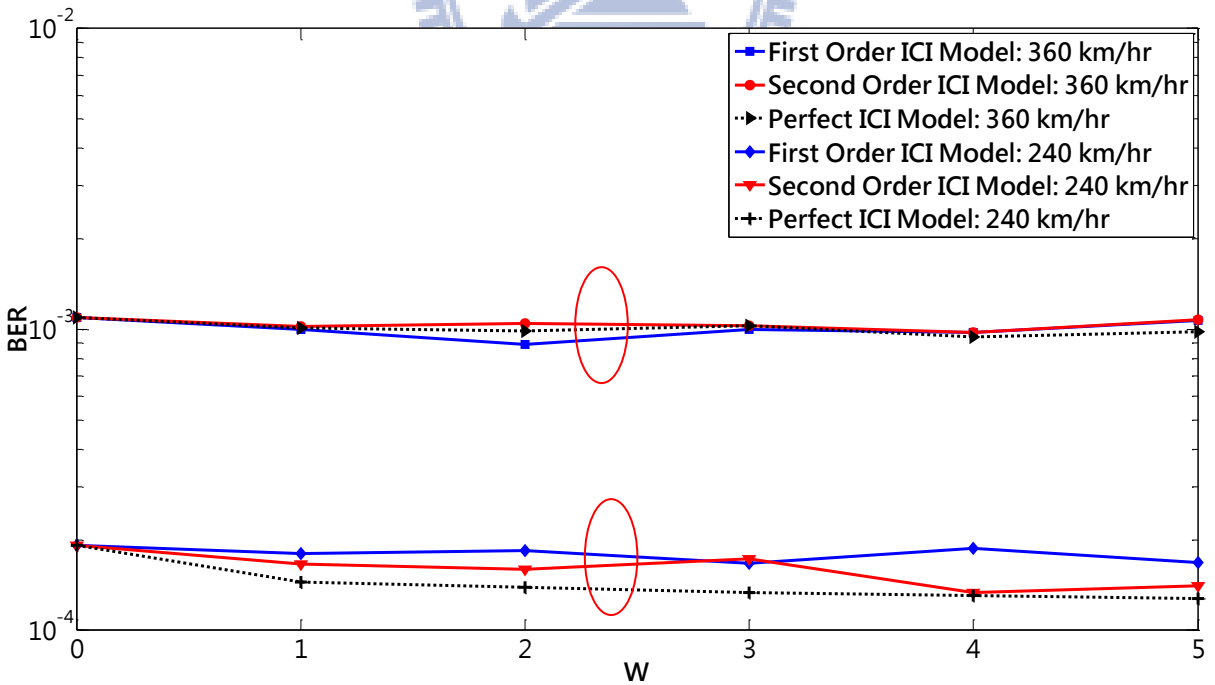

Fig.3.10 BER performances versus decoding iteration number for QPSK at vehicle speed 360 km/h and 240 km/hr

3.6.2 Proposed Decoding Scheme With Two-Stage Channel Estimator

By observing the simulations presented in Section3.6.1, we realize that the improvement of proposed algorithm becomes insignificant after the second decoding iteration. The improvement achieved by ICI cancellation saturates when $W > 2$, so we consider only the ICI caused by the four nearest four nearest subcarriers. Our proposed STBC-OFDM decoding scheme are presented in Fig.3.11 and Fig.3.12, where i and j stand for the iteration index of channel tracking and STBC decoding, respectively.

The software decoding scheme proposed in Fig.3.11 provides the best performance of our interference cancellation algorithm. Note that ICI cancellation is performed only at the last channel tracking update while CCI cancellation is performed since the second tracking iteration.

For hardware implementation, our clock cycle budget is very limited in the existed channel estimator hardware. The presented two-stage channel estimator was originally designed to employ four tracking iterations in the tracking stage, but it was simulated that the two-stage channel estimator has very similar performance between the 3^{rd} and 4^{th} tracking iteration. Therefore, we save one channel tracking iteration and perform interference cancellations only at the last channel tracking update. Our proposed hardware version STBC decoding is described in Fig.3.12.

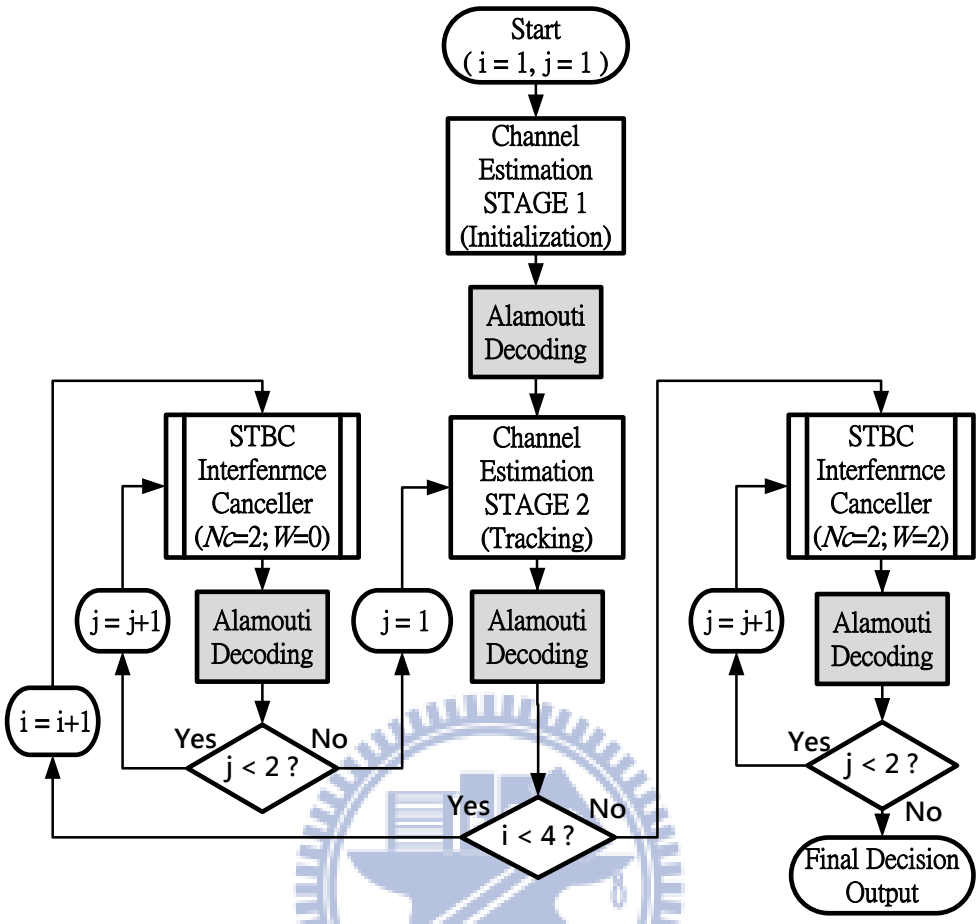

Fig.3.11 Proposed decoding scheme for software simulations (software version)

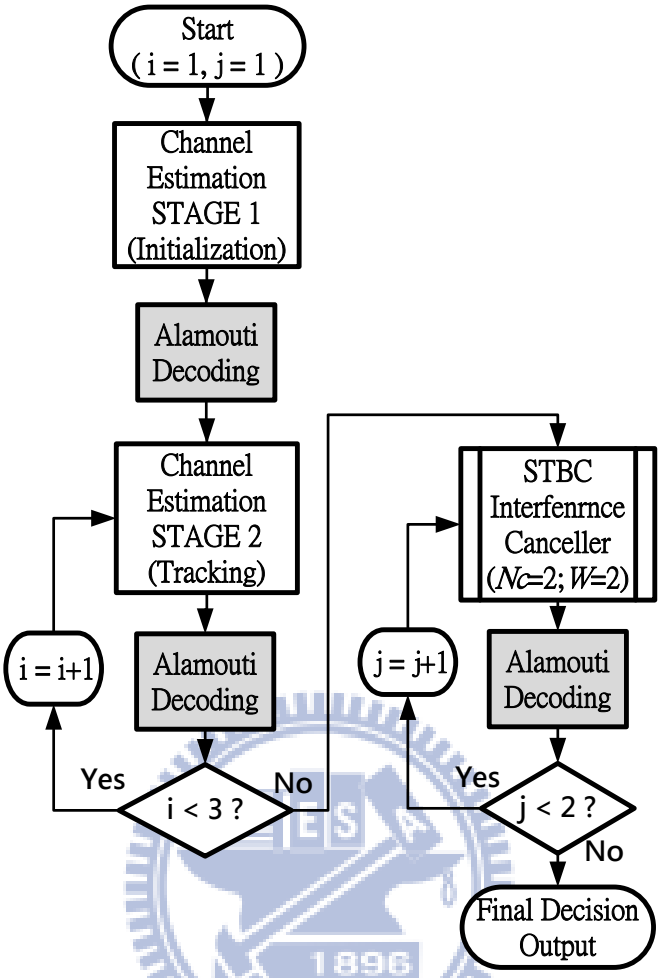

Fig.3.12 Proposed decoding scheme for hardware implementation (hardware version)

The performances of the proposed STBC interference canceller are demonstrated through the simulation of an STBC-OFDM system illustrated with the two stage DFT-based channel estimator introduced in Section 3.2. The following simulations uses perfect CSI at the receiver, and the STBC decoding flow is defined in Section 2.4. The multipath channel adopt the ITU Veh-A channel model with relative path power profiles of 0, -1, -9, -10, -15, and -20 (dB), and the path excess delays are uniformly distributed from 0 to 50 sampling periods. Jakes model is also used to generate Raleigh fading environment. Fig.3.13 – Fig.3.16 shows the BER versus Eb/No performances of different decoding scheme. The results of perfect channel estimation and perfect ICI model (W=2) are included as performance lower-bound. And several decoding schemes using perfect channel estimations are included as benchmarks. The notations of each decoding schemes are described in Table 3.3.

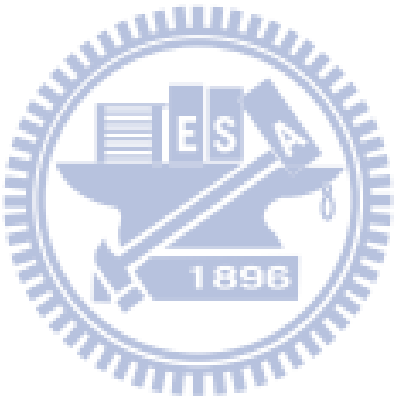

Table 3.3 Simulated Decoding Schemes

<table>
<tr><th>Scheme Notation</th><th>Channel Estimation</th><th>CCI cancellation</th><th>ICI cancellation</th></tr>
<tr><td>I0</td><td>perfect</td><td rowspan="2">non</td><td rowspan="4">non</td></tr>
<tr><td>T0
(original channel estimator design)</td><td>two-stage estimator
(4 tracking iterations)</td></tr>
<tr><td>I1</td><td>perfect</td><td>perfect</td></tr>
<tr><td>T1</td><td>two-stage estimator
(3 tracking iterations)</td><td>proposed algorithm</td></tr>
<tr><td>I2</td><td>perfect</td><td>perfect</td><td rowspan="3">1st order ICI model</td></tr>
<tr><td>T2
(hardware scheme)
(Fig.3.12)</td><td>two-stage estimator
(3 tracking iterations)</td><td rowspan="2">proposed algorithm</td></tr>
<tr><td>T3
(software scheme)
(Fig.3.11)</td><td>two-stage estimator
(4 tracking iterations)</td></tr>
<tr><td>P2
(benchmark)</td><td>perfect</td><td>perfect</td><td>perfect ICI model</td></tr>
</table>

Fig.3.13 shows the performance of 16QAM modulation at vehicle speed 240 km/hr. The two stage channel estimator provides very accurate CSI which performs almost equal to the perfect channel estimation, but the bounding floor at high SNR caused by interference noises is very distinct. With the aid of our proposed decoding scheme, the error floor of two-stage channel estimator significantly reduces by one order. BER of 2.6×10^{-3} can be achieved in Eb/No of 30dB. CCI cancellation contributes most of the improvement, it reduces BER from 1.5×10^{-2} to 3.6×10^{-3}. Then, ICI cancellation helps reduce about 6dB gap in Eb/No as compared with the perfect ICI model case at BER= 4×10^{-3}. As shown in Fig.3.14, in 16QAM

modulation and vehicle speed 360 km/hr. BER of 1.2×10^{-2} can be achieved in Eb/No of 30dB. Our proposed decoding scheme reduces the BER floor of two-stage channel estimator from 3.1×10^{-2} to 1.2×10^{-2}. And the gap between the case of perfect ICI model and proposed scheme with channel estimator is about 3dB in Eb/No at BER= 2×10^{-2}. As shown in Fig.3.15, in QPSK modulation and vehicle speed 240 km/hr. BER of 2.5×10^{-4} can be achieved in Eb/No of 30dB. Our proposed decoding scheme reduces the BER floor of two-stage channel estimator from 5.7×10^{-4} to 2.5×10^{-4}. And the gap between the case of perfect ICI model and proposed scheme with channel estimator is about 1.5dB in Eb/No at BER= 5×10^{-4}. As shown in Fig.3.16, in QPSK modulation and vehicle speed 360 km/hr. BER of 1.2×10^{-3} can bh11e achieved in Eb/No of 30dB. Our proposed decoding scheme reduces the BER floor of two-stage channel estimator from 2.3×10^{-3} to 1.2×10^{-3}, the gap between the case of perfect ICI model and proposed scheme with channel estimator is about 1.5dB in Eb/No at BER= 2×10^{-3}.

We should note that the error floor of perfect ICI model case at high SNR results from two reasons: the limitation of simple Alamouti decoding method and the ignored ICI noise from subcarriers outside of the range W. The limitation of Alamouti decoding method is the main reason, and several STBC data detection methods have been compared in [6].

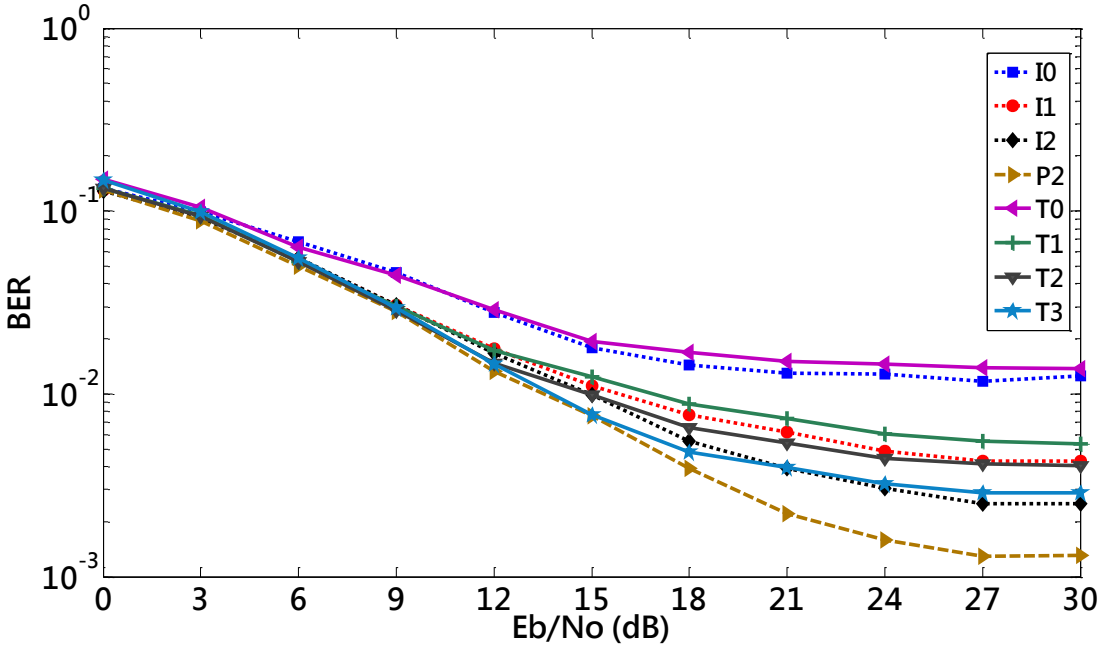

Fig.3.13 BER performance versus Eb/No for 16QAM at vehicle speed 240 km/hr

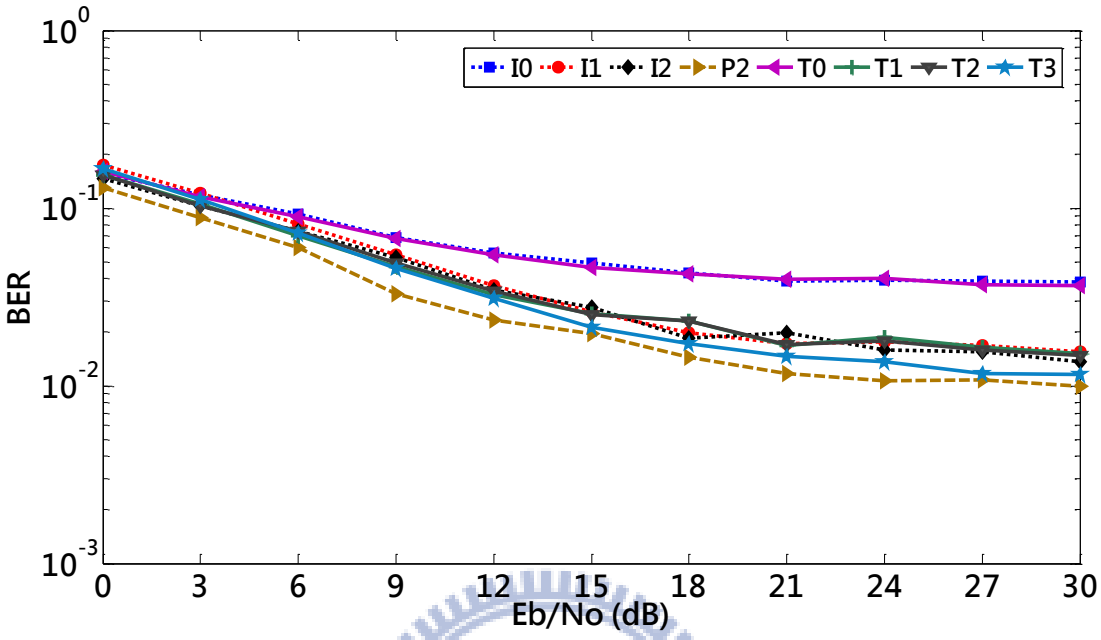

Fig.3.14 BER performance versus Eb/No for 16QAM at vehicle speed 360 km/hr

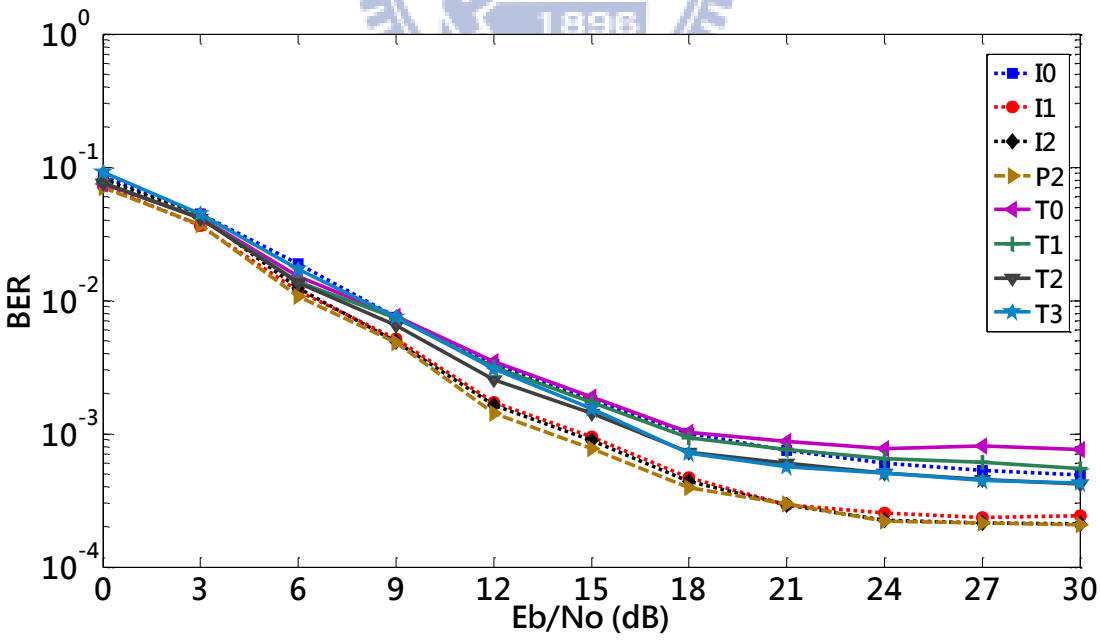

Fig.3.15 BER performance versus Eb/No for QPSK at vehicle speed 240 km/hr

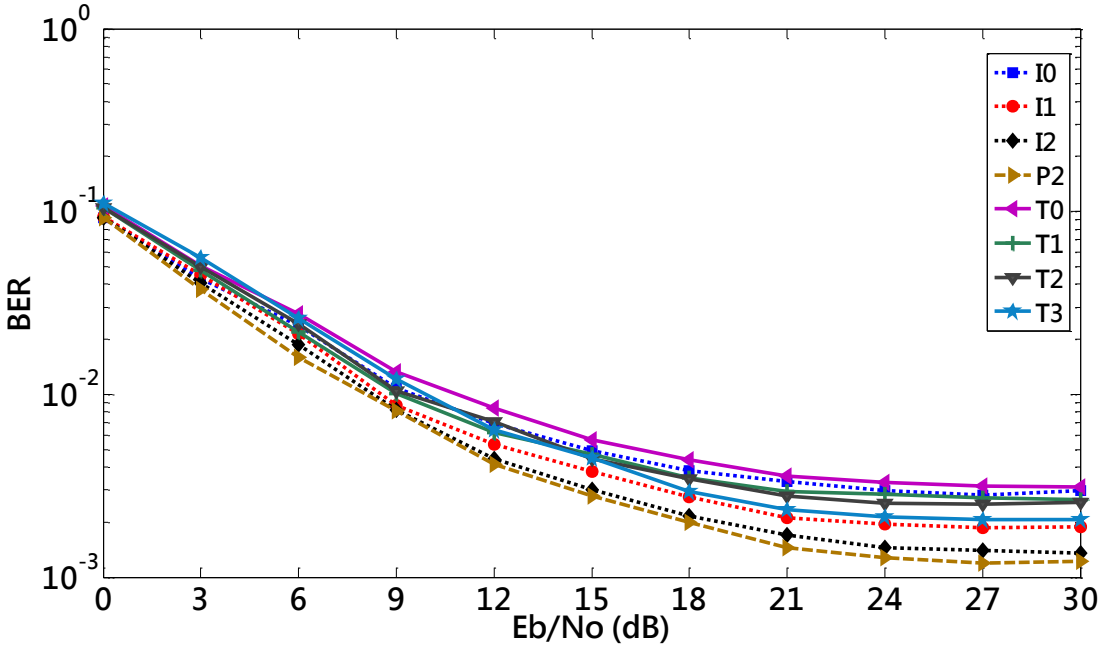

Fig.3.16 BER performance versus Eb/No for QPSK at vehicle speed 360 km/hr

3.7 Summary

In this chapter, an STBC interference canceller and a new decoding scheme for STBC-OFDM system are proposed to improve the previously studied two-stage channel estimator. The low complexity interference canceller exploits the existed symbol decisions and CFR estimations to cancel the interference noises introduced by Alamouti decoding method under time-varying multipath environment. As compared with the original channel estimator design, the improvement is very significant in high-QAM and high-vehicle speed condition. It can observed that 4 and 2.2 times improvement is achieved in BER for 16QAM modulation at vehicle speed of 240 and 360 km/hr, respectively. Moreover, the proposed STBC interference canceller provides an efficient solution for any conventional channel estimator designed for STBC-OFDM systems with very little overhead.

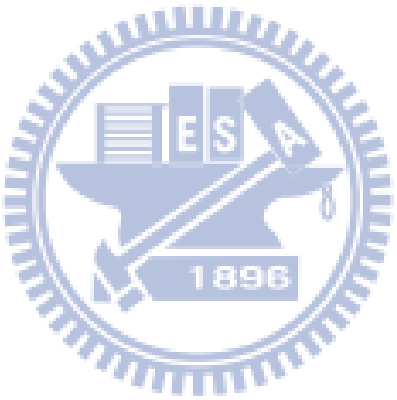

Chapter 4 Architecture Design and Circuit Implementation

According to our analysis and simulation, we proposed a STBC interference canceller architecture for 802.16e and 802.16m. To reduce the complexity of computation element, we adopt canonic sign digit (CSD) transform for those constant multiplications. And we written the equations to share common terms for those complex variable multiplications. Finally, we will present synthesis results.

4.1 Design Overview

The proposed STBC interference canceller is designed to have the following features:

- Provision of a low cost solution for improving STBC-OFDM system performance.
- Compatibility to any conventional STBC-OFDM system.
- Using only the existed results from channel estimator and STBC decoder, the increased hardware overhead is trivial.

The implementation were optimized for cooperating with the two-stage channel estimator introduced in Section 3.2.2

Fig.4.1 shows the architecture of the proposed STBC interference canceller with the two stage channel estimator. The main computations of our proposed interference model, (3.31)-(3.32), are separated into two parts, the STBC re-encoder and the shaping filter. The STBC re-encoder exploits the channel estimations and decision symbols to estimate the variation of the interference-free and AWGN-free received signals at one certain transmit subcarrier between two time slots. Based on the received signal variation of a certain subcarrier, the shaping filter approximates the CCI noise induced to this subcarrier and the ICI noise spread

to other subcarriers. Then, the shaping filter accumulats the interference noise of a received subcarrier from other transmit subcarriers. Finally, the estimated interference is cancelled from the actual received signal and put the cleaner received signal into the STBC decoder to generate better decision symbols.

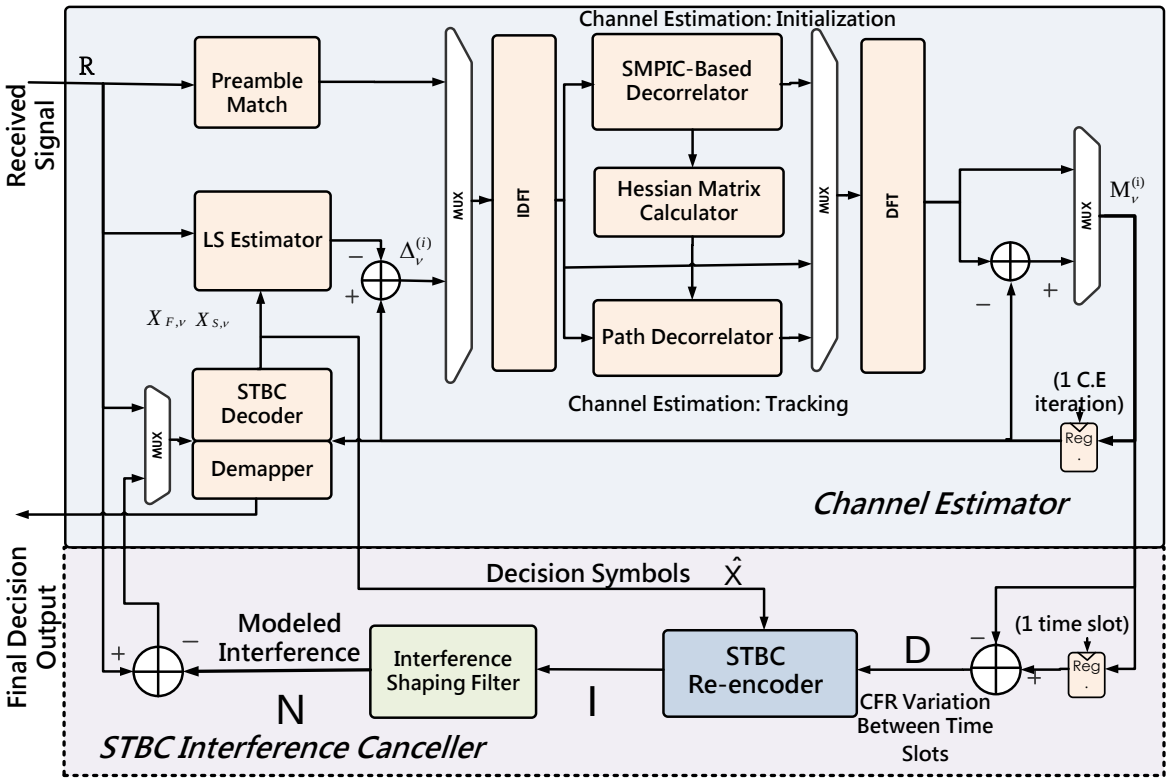

Fig.4.1 Block diagram of the proposed STB interference canceller with the two stage channel estimator

Blocks like the memory used to store the latest CFR estimation, the memory holds the received signals, the pilot read-only memory (ROM), the STBC decoder, and the demapper. are shared with the existed channel estimator implementation [3]. The proposed architecture is shown in Fig.4.1, and the signal processing clow is presented in Fig.4.3. The memory labeled as “Previous CFR Mem.” records the CFR estimations of the last channel tracking stage iteration before a new initialization stage begins. A dual port data decision memory is a which enables one read and one write to different entries simultaneously. Shaded blocks in Fig.4.3 are the overhead of my implementation, while other white blocks can be shared with the existed

channel estimator hardware.

Since the constellation values are known, we store the demapped binary bit value of decision symbols instead of their complex value to save memory size. The constellation mapper read the binary bit value stored in data decision memory or pilot ROM, and convert it into complex value. Note some common multiplications between (3.31) and (3.32) can be shared, so we integrate the computation of pilot ICI component into the STBC re-encoder and select the output according to the status of the f -th subcarrier, where the subcarrier index $f \in \{\{\mathbf{J} \cup \mathbf{\Theta}\}, 0\}$ is chosen to skip guard band.

Assuming that $2w$ neighboring subcarriers induce significant ICI noise into the central subcarrier, the shaping filter computes the interference noise to the subcarriers among $(f+w)$ -th and $(f-w)$-th received subcarrier which are caused by the f -th transmitted subcarrier. After the $2w$ interference noise sources ahead of the $(f-w)$-th received subcarrier are accumulated, we obtain the total approximated interference noise at the $(f-w)$-th received subcarrier. The calculated interference noise is cancelled from the $(f-w)$-th received for an new symbol decision.

The finite state machine (FSM) and state behavior description are described in Fig.4.2 and Table3.1, respectively.

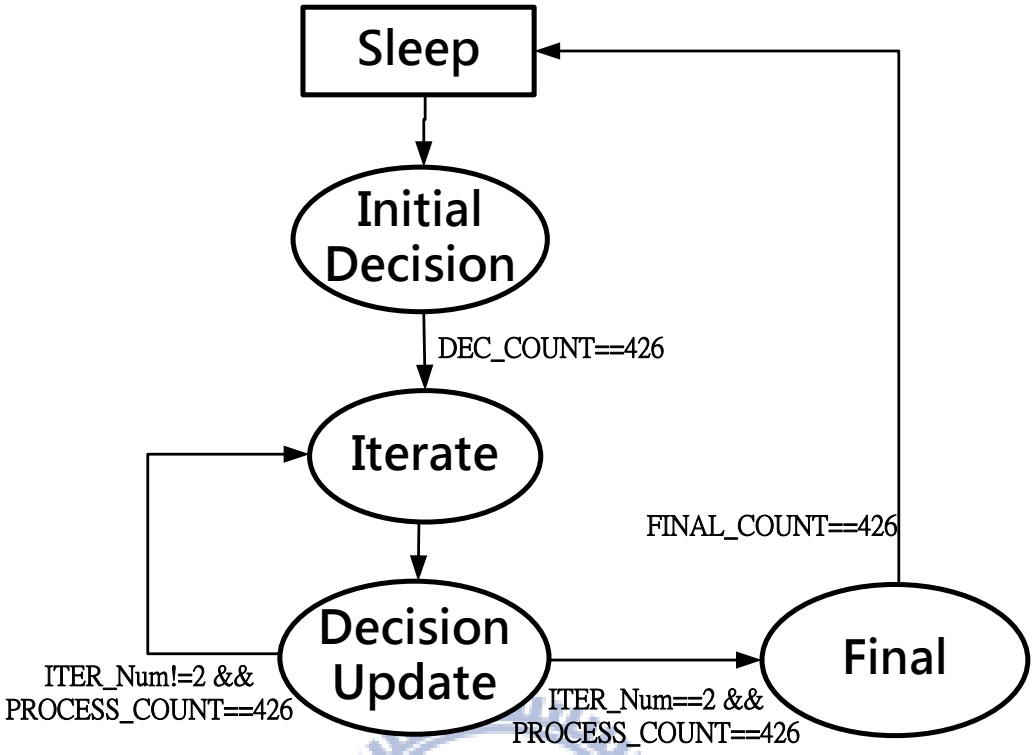

Fig.4.2 State transition diagram of the proposed STBC interference canceller

Table 4.1 State definitions of proposed STBC interference canceller

State Name	State Behavior
Sleep	Disable all memory access and read.
Iterate	Reset status registers and begin a new decoding iteration.
Initial Decision	Current subcarrier is a data subcarrier, read STBC re-encoder input symbol from decision symbol memory.
Decision Update	Apply the proposed STBC interference cancellation algorithm and update decision symbols.
Final	All decode iterations are done, output the final decision data sequence.

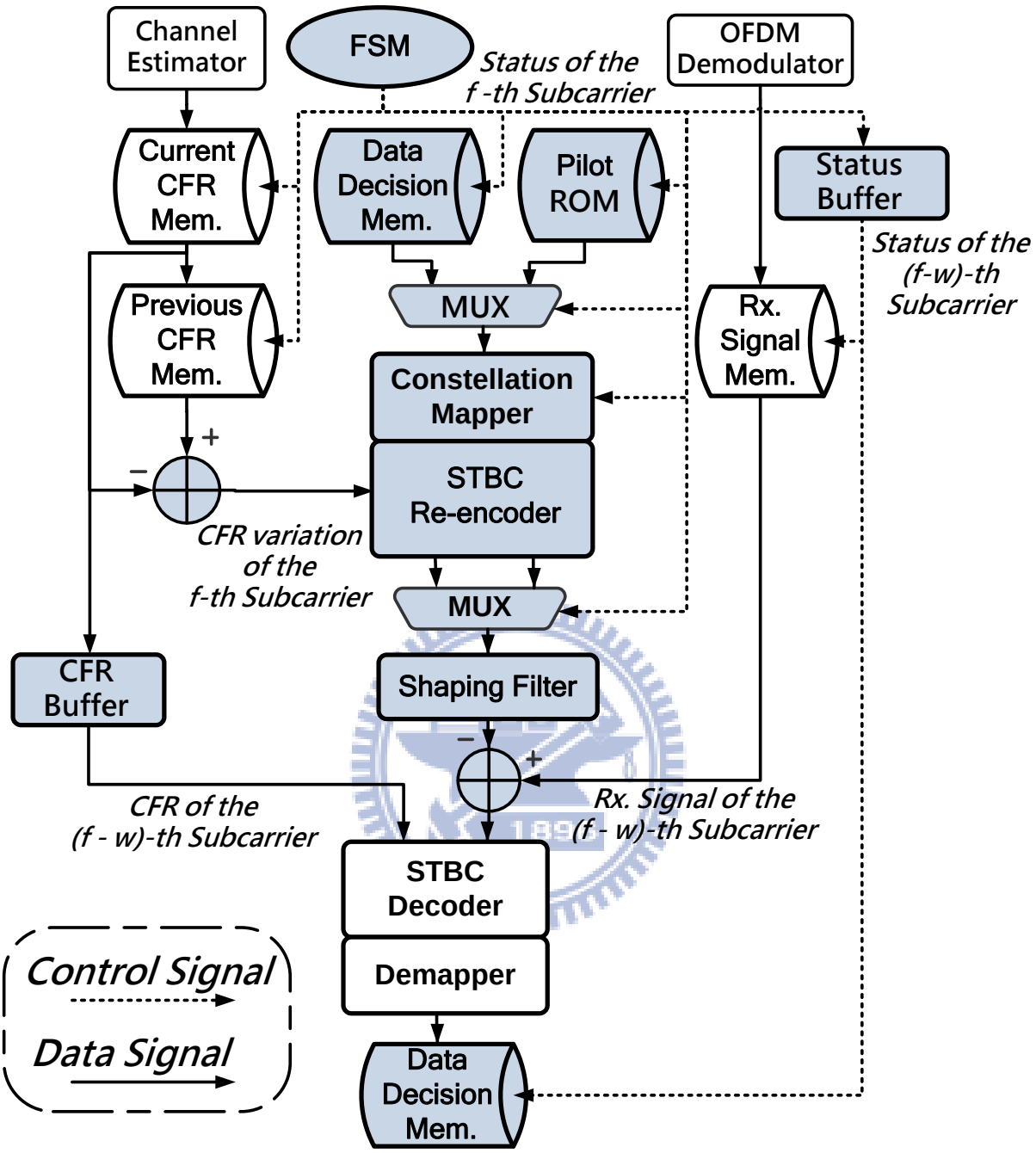

Fig.4.3 Architecture of the proposed STBC interference canceller

4.2 Word Length Optimization

Word length in hardware implementation determines signal precision, because its truncating operation is equivalent to adding quantization noise into signals. To achieve better system performance, one would prefer longer word length. But longer word length will increase hardware complexity, increase combinational logic delay, and consume more power. Therefore, it is important to reduce word length as much as possible and maintain the acceptable system performance.

The word length contains integer part and fractional parts. We deter a minimum length of the integer part to guarantee that the signal does not overflow during computation. As for the fractional part, we use output SNR at the final decision symbols as a guide of system performance to determine the word length at the input and output of each function block defined in Fig.4.1, and the equations are given by

$$\begin{aligned} output\ SNR &= \left(\sum_{p=0}^{N_{QAM}-1} SNR_p \cdot n_p \right) \Big/ \left(\sum_{p=0}^{N_{QAM}-1} n_p \right) \\ SNR_p &= 10log_{10}\left(\frac{\phi_p^2}{2\sigma_p^2} \right) \\ \phi_p &= \frac{1}{n_p} \sum_{j=0}^{n_p-1} \left| X_j \right| \\ \sigma_p^2 &= \frac{1}{n_p - 1} \sum_{j=0}^{n_p-1} \left(\left| X_j \right|^2 - \left| \phi_p \right|^2 \right) \end{aligned} \tag{4.1}$$

where N_{QAM} is the number of symbols in a constellation, n_p is the number of data belong to the p-th symbol after sliced, and X_j is the decided data after STBC decoding.

Fig.4.5. shows the curve of the output SNR versus different fractional part word lengths for the output of the shaping filter output.

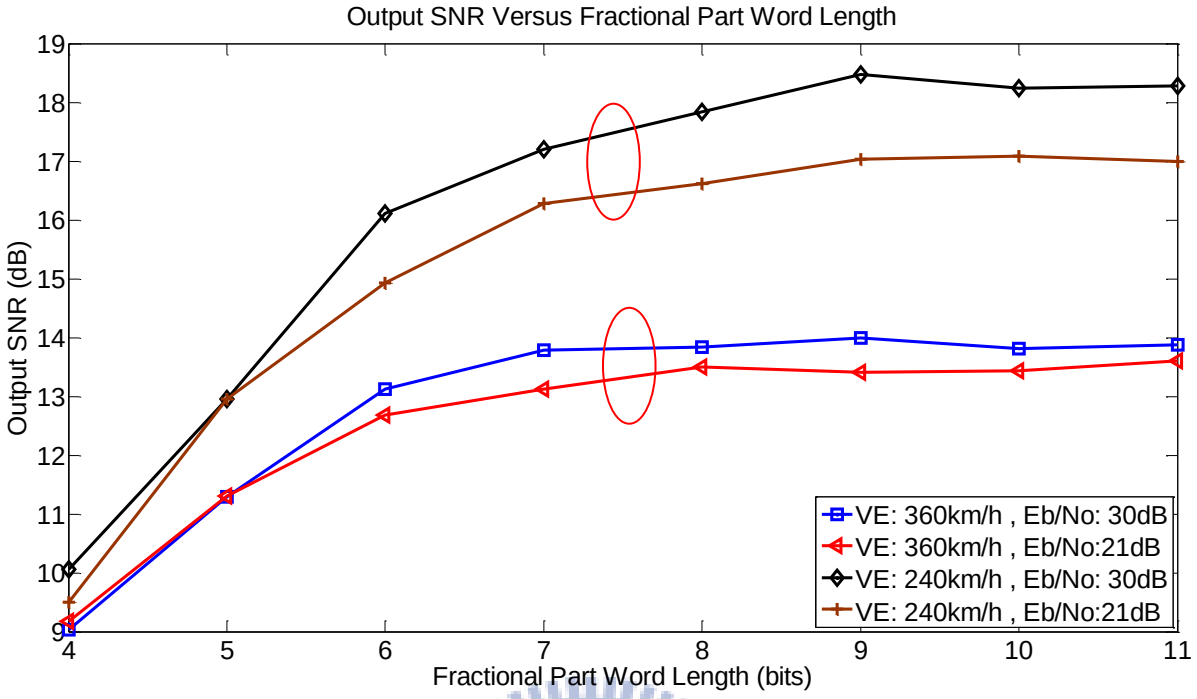

Fig.4.4 Output SNR versus different fractional part word lengths for the shaping filter output

These curves are simulated at vehicle speed of 240 km/h with different $E_b/N_0\,(dB)$. The fractional part of word length is decided to be 9 where the output SNR starts getting saturated. The word lengths of several key signals are summarized in Table 3.2.

Table 4.2 Word lengths of several key signals in the proposed STBC interference canceller

Signal	Word Length	
	Integer Part	Fractional Part
Stored Previous CFR	2	6
CFR Variation Between Two Time Slots	2	6
Decision Symbol Input of Re-encoder	5	5
Output of Re-encoder	3	7
Output of Shaping Filter	2	9
Updated Received Signal	3	10

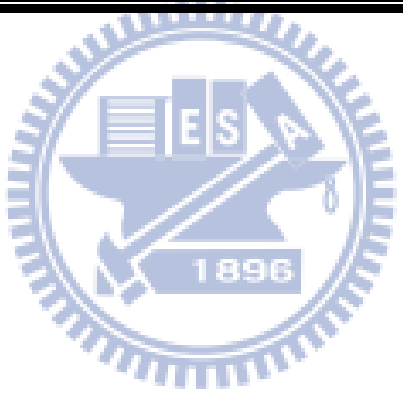

4.3 STBC Re-encoder Block

The STBC re-encoder reconstructs the interference-free and AWGN-free received signals variation between current and previous time slot at the f -th subcarrier. Both pilot and data subcarriers are considered, and the outputs are selected according to the subcarrier status of the input signals. Each of the complex multiplication involved in (3.30)-(3.31) needs four multiplications and two additions if we realize it directly,

$$(A+jB)\times(C+jD)=(AC+BD)+j(BC-AD) \tag{4.2}$$

However, many schemes that use less number of multiplication has been studied in [21]. They also claim the follow realization form requires only three multiplications while maintains the same truncation noise energy as (4.2):

$$(A+jB)\times(C+jD)=\left[(A-B)C+A(C-D)\right]+j\left[(A-B)C+B(C+D)\right] \tag{4.3}$$

Our proposed design of STBC re-encoder is shown in Fig.4.5, which contains twelve multipliers and twenty adders. The shaded twelve adders or subtractors are the overhead of saving four multipliers, and the shaded multipliers are used to generate the common term (A-B)C in equation (4.3).

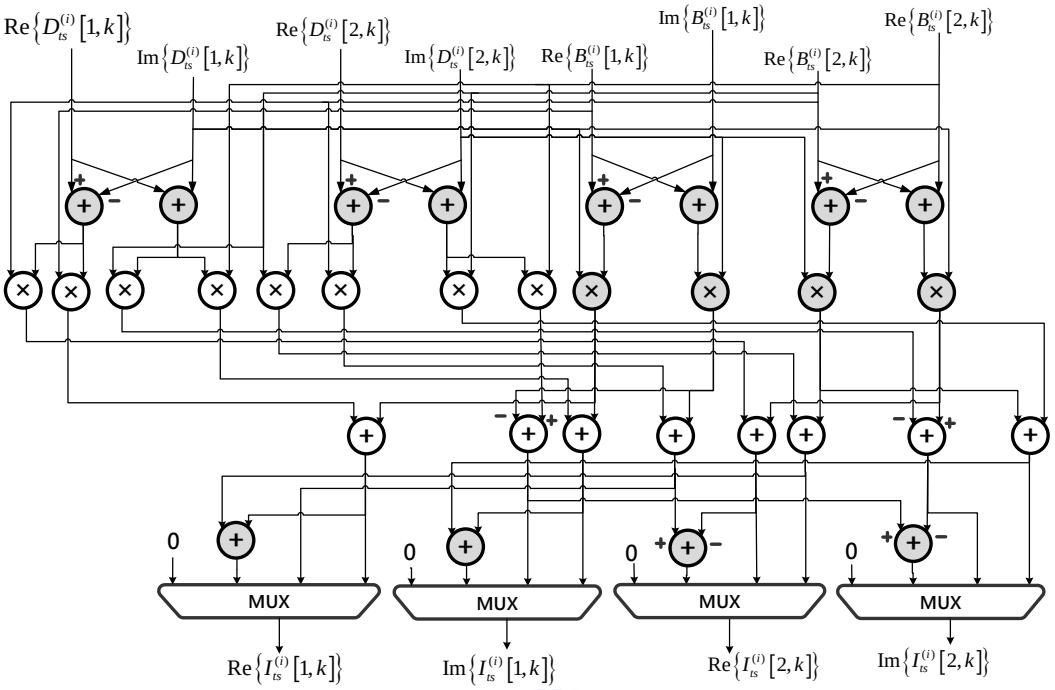

Fig.4.5 STBC re-encoder circuit design

4.4 Interference Shaping Filter Block

The interference shaping filter contains constant complex coefficients and a set of accumulating register. From the simulation results presented in Section 3.6.1 we realize that the improvement achieved by ICI cancellation saturates when $W > 2$, that is we should only consider the ICI from nearest four subcarriers and set $W = 2$. We approximate Doppler spread and CCI noise by multiplying the precomputed coefficients $S_b\left[\left|w\right|\right]$, which are described in (3.29), with the variation of noise-free received signal reconstructed by STBC re-encoder. We apply CSD coding on the coefficients S_b to minimize the number of addition needed. As a result, the complex multiplications involved inside the interference shaping filter are implemented using only several adders, as illustrated in Fig.4.6 (a) and (b). The shift registers accumulate the ICI noises from $2W$ neighboring subcarriers and the CCI noise from the same subcarrier. When the input is the reconstructed interference-free received signal of subcarrier f , the output of interference shaping filter is the total interference noise at received subcarrier $f-2$.

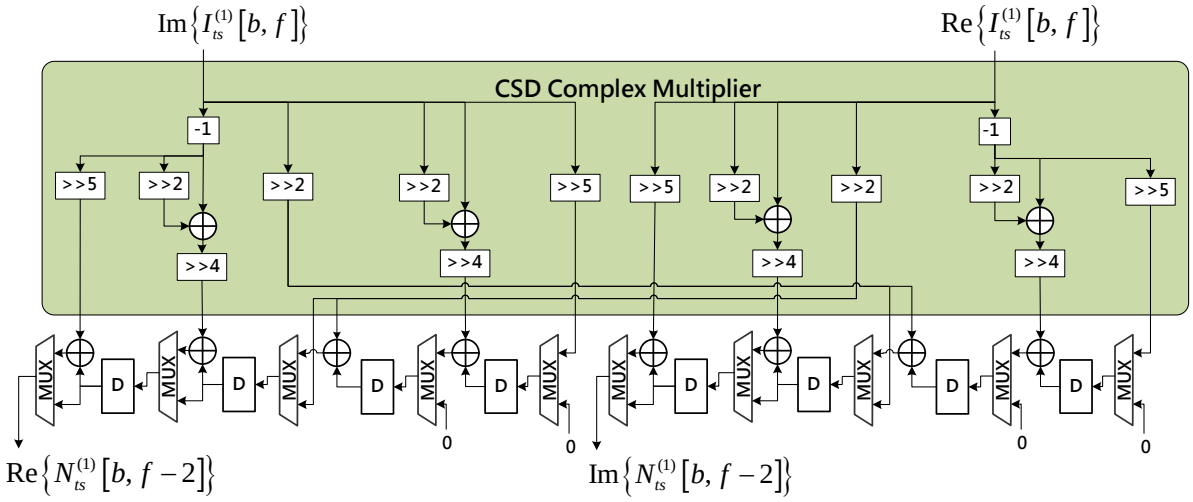

(a)

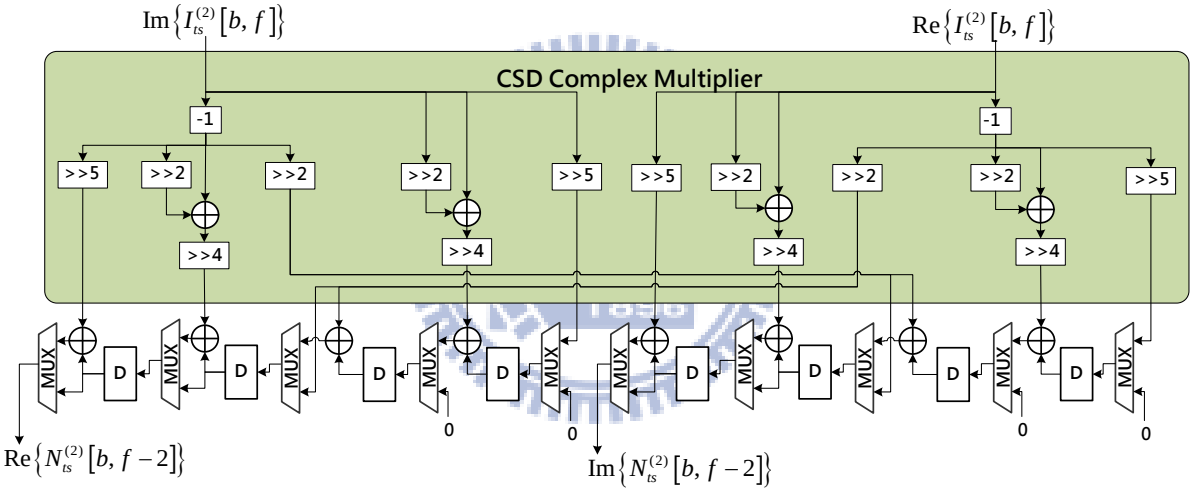

(b)

Fig.4.6 Design of shaping filter circuit design of (a) the first transmit antenna branch and (b) the second transmit antenna branch

4.5 Simulation Results

The performances of the proposed STBC interference canceller are demonstrated through the simulation of an STBC-OFDM system with the two stage DFT-based channel estimator introduced in Section 3.2. The STBC decoding flow is defined in Section 2.4. The multipath channel adopt the ITU Veh-A channel model with relative path power profiles of 0, -1, -9, -10, -15, and -20 (dB), and the path excess delays are uniformly distributed from 0 to 50 sampling periods. Jakes model is also used to generate Raleigh fading environment. Fig.3.12 – Fig.3.15 shows the BER versus Eb/No performances of different decoding scheme under QPSK modulation or 16QAM modulation at vehicle speed of 360 km/hr or 240 km/hr. The results of perfect channel estimation and perfect ICI model (W=2) are included as benchmarks, denoted as "P2". The maximum Doppler f_d is 555.6 Hz and the normalized Doppler is 0.05 for vehicle speed 240 km/hr, similarly $f_d = 833.4$ Hz and $f_d / \Delta f = 0.075$ for vehicle speed 360 km/hr. "T2" denotes the floating point performance of proposed decoding scheme. The hardware version performance of "T2" scheme is simulated with fixed-point word length and denoted as "F2". The curves of proposed scheme and the hardware version are very close. The detail of each "T2" and " P2" scheme are described in Table 3.3.

As shown in Fig.4.7, in 16QAM modulation and vehicle speed 240 km/hr, the curve of the hardware version has about 0.5 dB gap in Eb/No as compared with proposed scheme and 1 dB gap as compared with perfect ICI model case at BER= 5×10^{-3}. As shown in Fig.4.8, in 16QAM modulation and vehicle speed 360 km/hr, the curve of the hardware version has about 0.7 dB gap in Eb/No as compared with proposed scheme and 2.5 dB gap as compared with perfect ICI model case at BER= 3×10^{-2}. As shown in Fig.4.7, in QPSK modulation and vehicle speed 240 km/hr, the curve of the hardware version has about 0.5 dB gap in Eb/No as compared with proposed scheme and 1 dB gap as compared with perfect ICI model case at BER= 10^{-3}. As shown in Fig.4.8, in QPSK modulation and vehicle speed 360 km/hr, the curve of the hardware version has about 0.7 dB gap in Eb/No as compared with proposed scheme and 1 dB gap as compared with perfect ICI model case at BER= 5×10^{-3}.

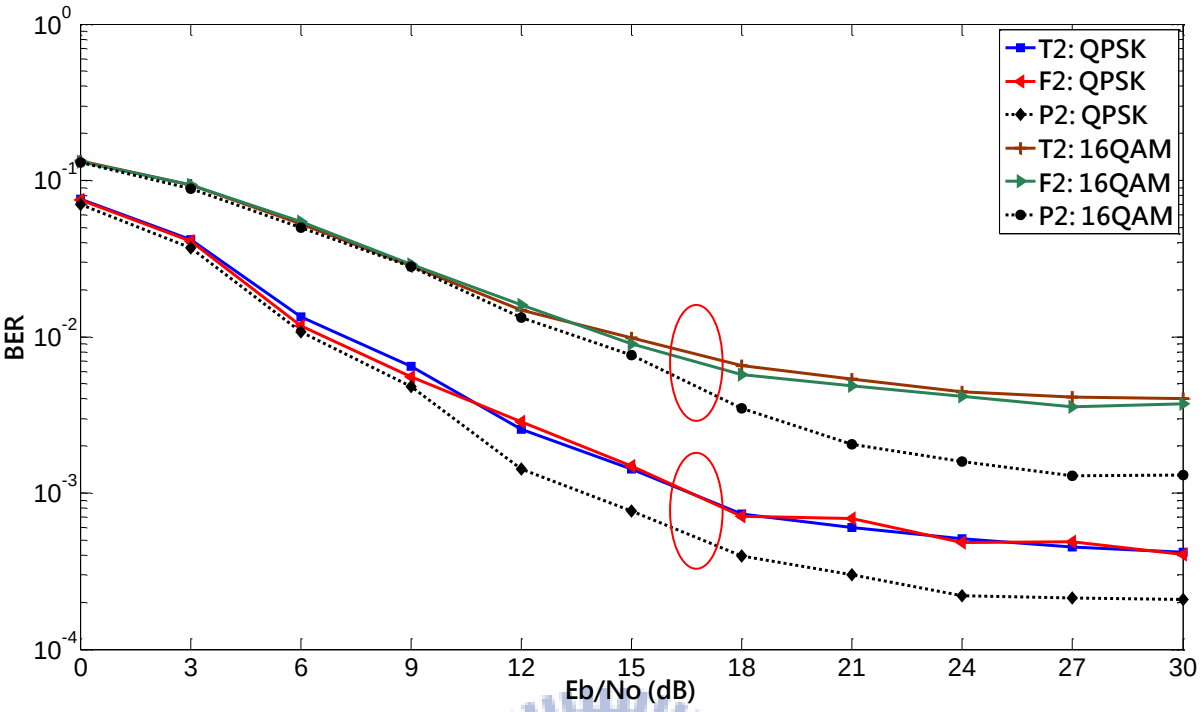

Fig.4.7 BER performance versus Eb/No at vehicle speed 240 km/hr

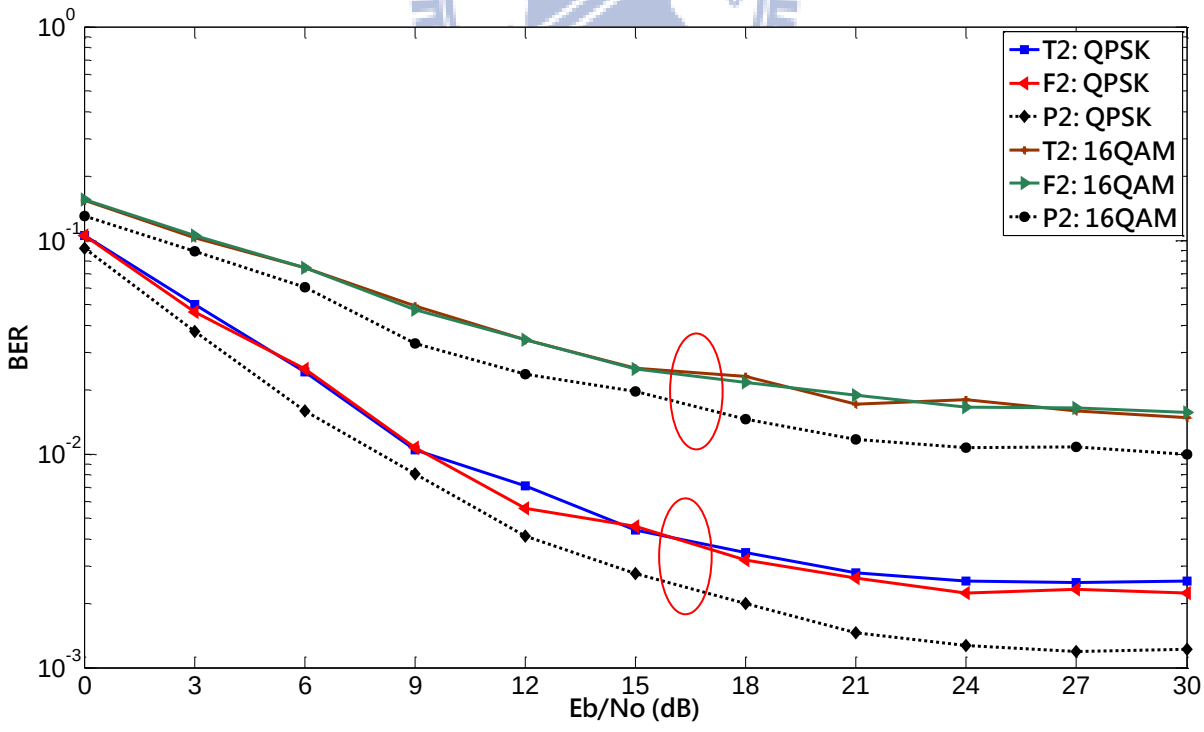

Fig.4.8 BER performance versus Eb/No at vehicle speed 360 km/hr

We use the improved performance ratios to demonstrated the improvement of proposed STBC interference canceller, which are given by

$$\begin{aligned}
&\text{Improved Performance Ratio of } F2 = \frac{\text{BER of } T0}{\text{BER of } F2} \\
&\text{Improved Performance Ratio of } I2 = \frac{\text{BER of } I0}{\text{BER of } I2} \\
&\text{Improved Performance Ratio of } P2 = \frac{\text{BER of } I0}{\text{BER of } P2}
\end{aligned} \tag{4.4}$$

Fig.4.9 shows the improved performance of 16QAM at vehicle speed 240 km/hr. Nearly 5 time improvement can be achieved if perfect channel estimation is applied to our proposed decoding scheme. Our proposed interference canceller and two-stage channel estimator implementation provides 3.9 and 2.2 time improvement in Eb/No of 15 and 30 dB, respectively. Fig.4.10 shows the improved performance of 16QAM at vehicle speed 360 km/hr. 2.8 time improvement can be achieved if perfect channel estimation is applied to our proposed decoding scheme. Our proposed interference canceller and two-stage channel estimator implementation provides 2.4 and 1.9 time improvement in Eb/No of 15 and 30 dB, respectively.

Fig.4.11 and Fig.4.12 shows the improved performance of QPSK modulation at vehicle speed of 240 km/hr and 360 km/hr, respectively. The improvements of our proposed implementation do not exceed 2 times. This is because QPSK modulation has better resolution and is more robust compared to 16QAM modulation, the effect of STBC interference noses are not significant. As a result, the modeling error of our proposed algorithm counteracts the cancelled interference noise and results in limited performance improvement.

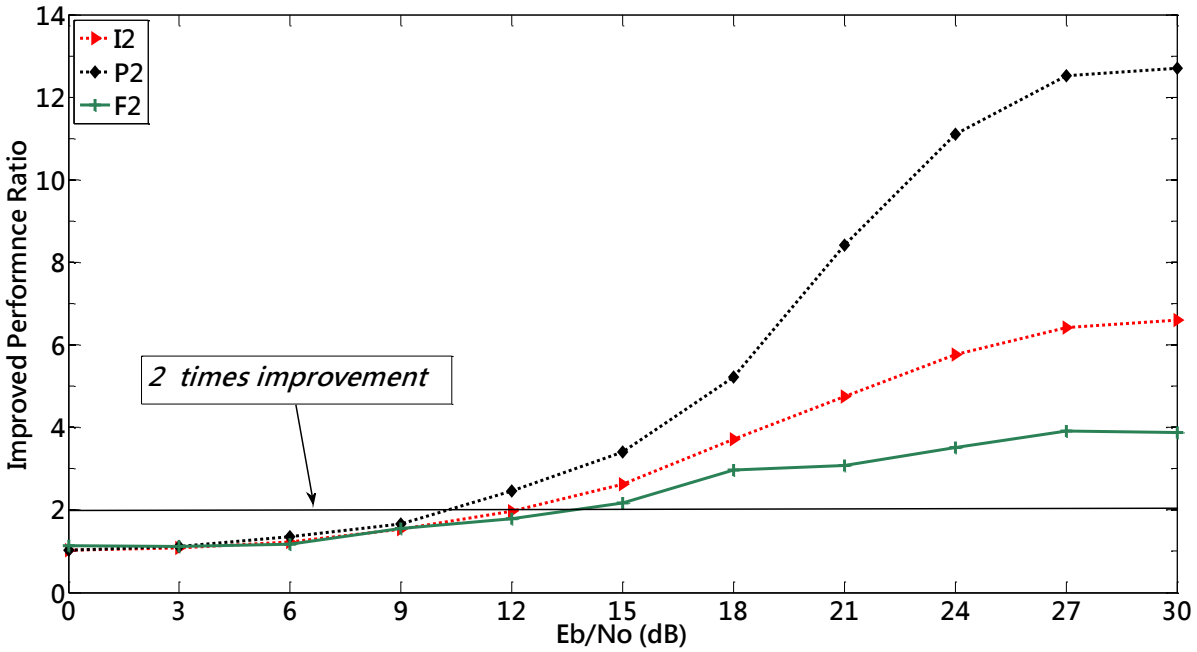

Fig.4.9 Improved performance ratio of 16QAM at vehicle speed 240 km/hr

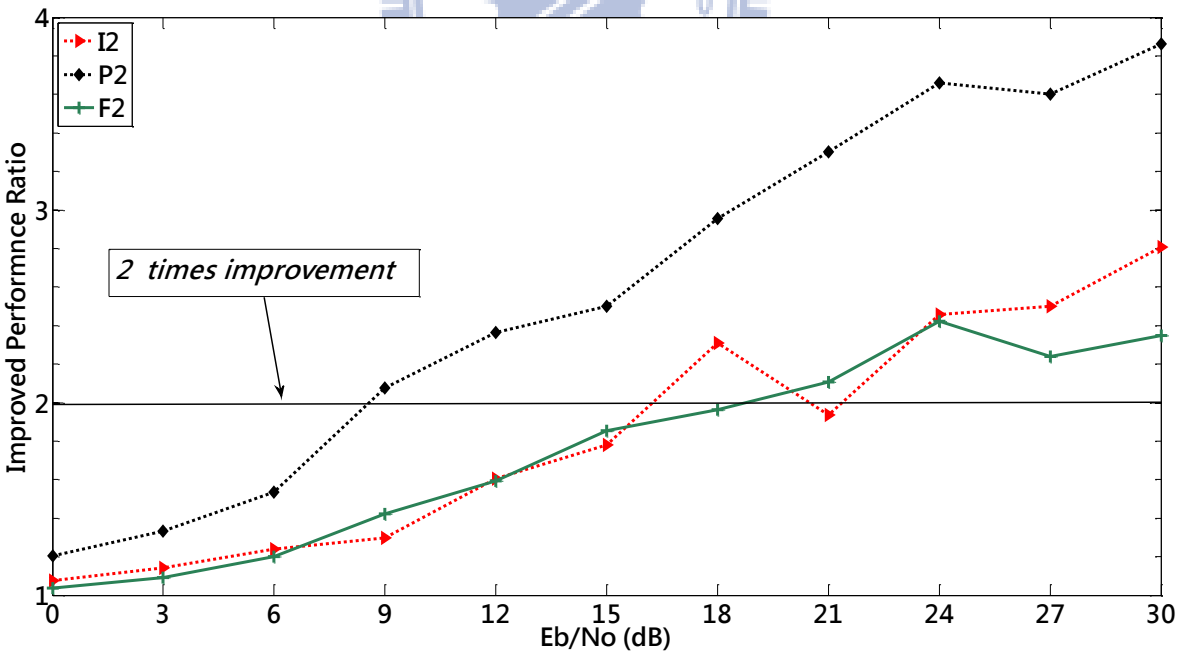

Fig.4.10 Improved performance ratio of 16QAM at vehicle speed 360 km/hr

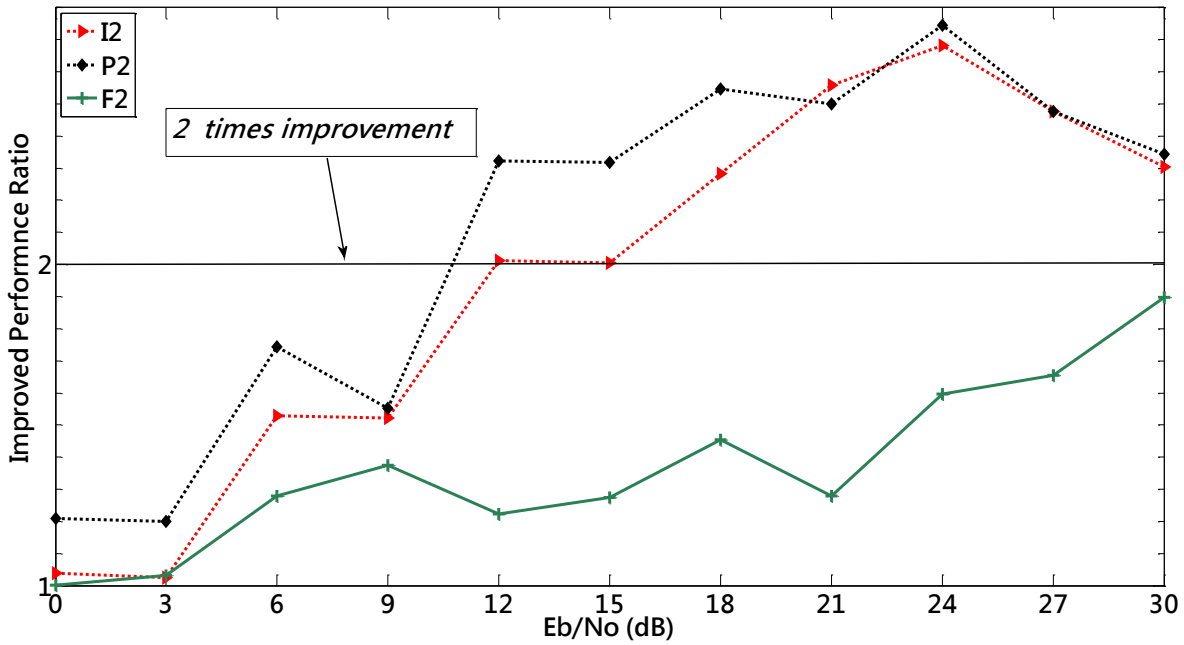

Fig.4.11 Improved performance ratio of QPSK at vehicle speed 240 km/hr

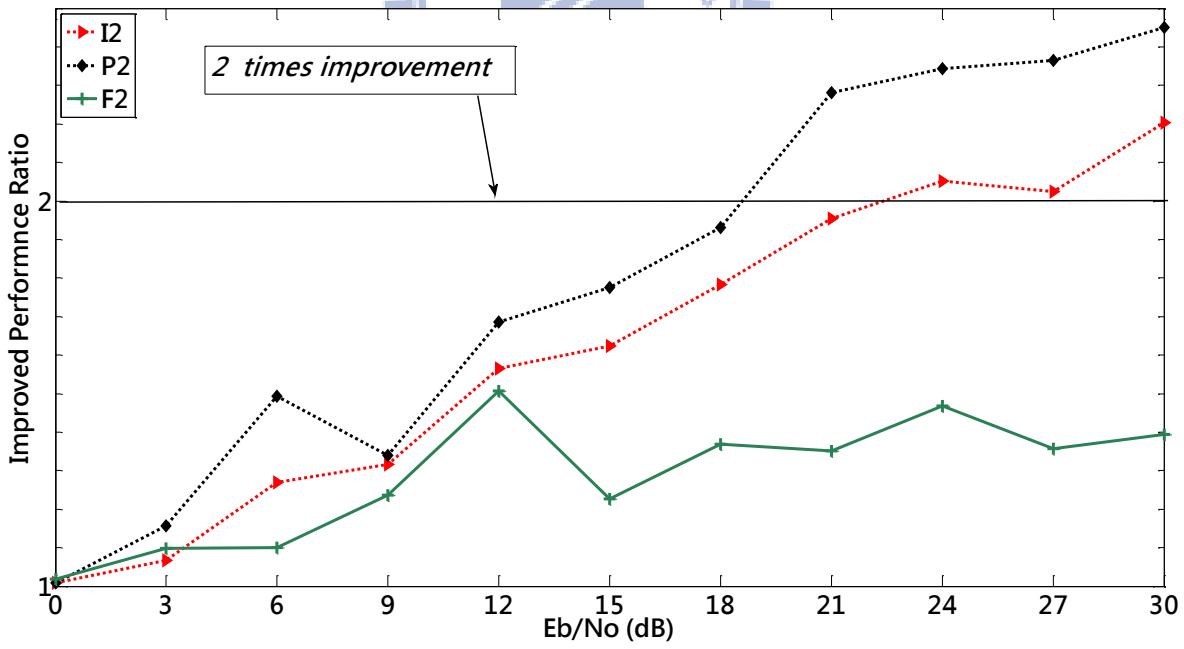

Fig.4.12 Improved performance ratio of QPSK at vehicle speed 360 km/hr

4.6 Design Results

The proposed STBC interference canceller is implemented in 90 nm 1P9M, 1V CMOS technology. The synthesis results are listed in Table 4.3. The area is 0.44 mm^2 and equivalent to 109,299 gates. The OFDM receiver samples received signal at 11.2 MHz , and the STBC interference canceller operates at 78.4 MHz. The power is equivalent to 1.45 mW from a supply voltage 1 V.

Table 4.3 Synthesis Result of Proposed STBC Interference Canceller

Technology	CMOS 90nm 1P9M, 1V
Sampling Frequency	11.2 MHz
Clock Frequency	78.4 MHz
Gate Counts including SRAM	109,299 gates (0.44 mm^2)
SRAM Size	140.93 K bits
Power	1.45 mW
Overhead of Proposed STBC Interference Canceller	
Gate Counts including SRAM	42,277 gates (0.083 mm^2)
SRAM Size	22.14 K bits

The ratio of combinational and non-combinational area is about 1:4; in other word, the use of memory in this design occupies about 80% of overall design. Note that the STBC decoder, the demapper, the received signal memories, and the memories storing the latest CFR estimations are shared with two-stage channel estimator. The overhead of our proposed

Interference canceller are the STBC re-encoder, the shaping filter, the dual-port decision symbol memory, and the single port memories used to store the CFR estimations of previous time slot. As shown in Fig. 4.13, the STBC re-encoder and shaping filter take 11% of the Interference canceller, and the overhead memories take 28%. Up to 61% of hardware is shared with the existed two-stage channel estimator hardware. As implemented in [3], the total gate count of the two-stage channel estimator excluding the FFT/IFFT module is 859,604. Our proposed STBC interference canceller takes only 4.9% of the channel estimator.

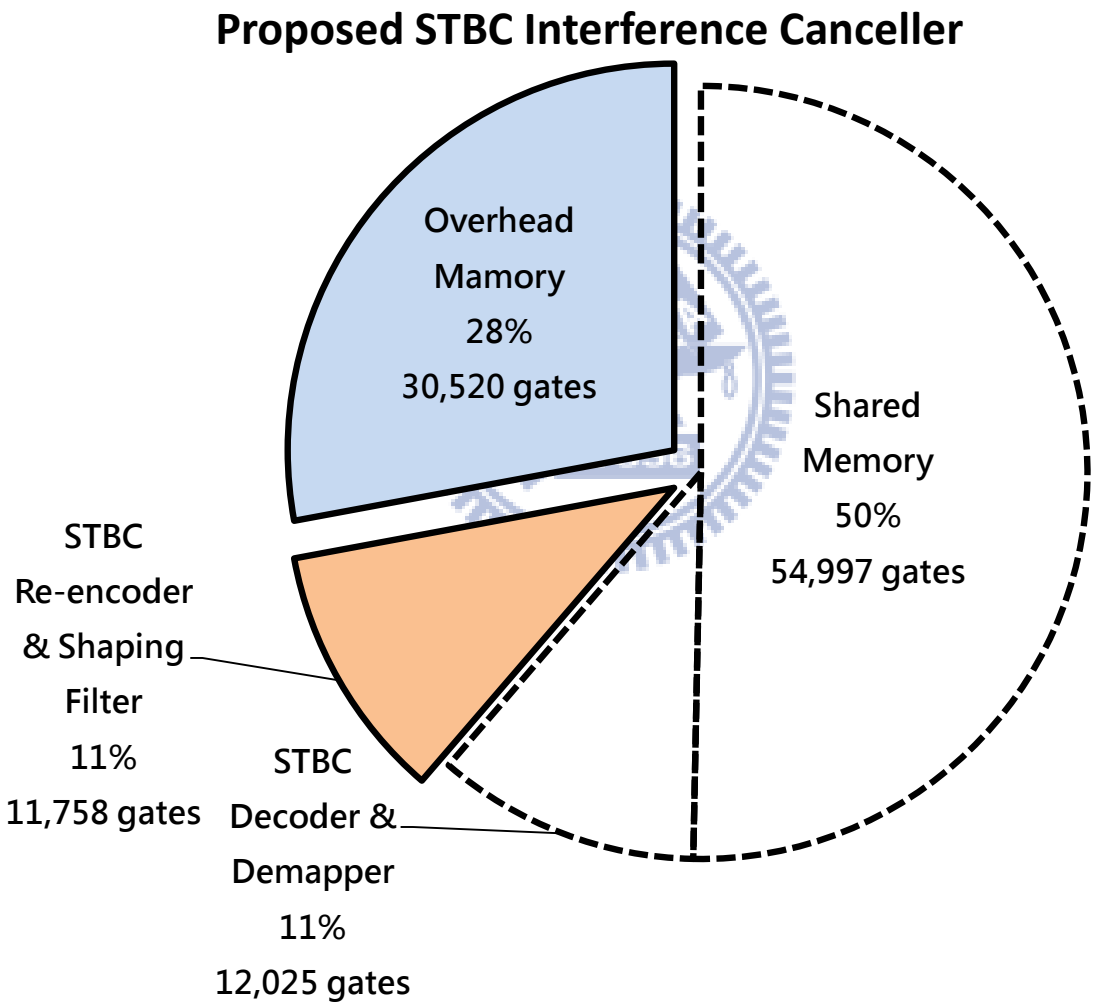

Fig. 4.13 Area proportion of the proposed STBC Interference Canceller

Chapter 5 Conclusion

In this thesis, first, an STBC interference cancellation algorithm for ICI and CCI is proposed then, we implement an efficient STBC interference canceller for OFDM receiver in outdoor mobile channels. The proposed joined ICI and CCI canceller is successfully applied in an existed IEEE802.16e STBC-OFDM receiver and can easily be adapted into IEEE802.16m STBC-OFDM receiver, too. Features of the proposed STBC interference canceller are

- development of an low complexity interference cancellation algorithm for any STBC-OFDM system with two transmit antennas and one receive antenna to improve system performance;
- implementation of an efficient STBC interference canceller;
- integration of the proposed STBC interference canceller with a two-stage channel estimator at about 4.9% overhead cost;

From the system simulation results, we have shown that more than 2 times BER improvement for 16QAM modulation at the vehicle speed 360 km/hr with Eb/No beyond 15dB. In 16QAM modulation at the vehicle speed of 240 km/hr with Eb/No over 15dB, BER decreases from 10^{-2} to 10^{-3} without using channel coding. The design of the proposed STBC interference canceller has an equivalent gate count of 109,299 gates, 61% of which can be shared with the tow-stage channel estimator. The synthesis result dissipates 1.45 mW at 78.4 MHz operating frequency using 1V supply voltage supply and 90 nm CMOS technology. With verifications through design and simulation results, the proposed STBC interference canceller can provide an performance-improving solution for STBC-OFDM baseband receivers in WMAN mobile wireless communication.

References

[1] *IEEE Standard for Local and Metropolitan Area Networks Part 16: Air Interface for Fixed and Mobile Broadband Wireless Access Systems Amendment 2: Physical and Medium Access Control Layers for Combined Fixed and Mobile Operation in Licensed Bands and Corrigendum 1*, IEEE Std 802.16e-2005, pp. 1-822.

[2] *IEEE Draft Amendment Standard for Local and Metropolitan Area Networks - Part 16: Air Interface for Broadband Wireless Access Systems - Advanced Air Interface*, IEEE P802.16m/D8, August 2010,

[3] H. Y. Chen, M. L. Ku, S. J. Jou and C. C. Huang, "A Robust Channel Estimator for High-Mobility STBC-OFDM Systems," *IEEE Trans.Circuits Syst. I, Reg. Papers,* vol. 57, no.4,pp. 925-936, Apr. 2010.

[4] W. G. Jeon, K. H. Chang and Y. S. Cho"An equalization technique for orthogonal frequency-division multiplexing systems in time-variant multipath channels," *IEEE Trans. Commun.,* vol. 47,no.1, pp. 27-32, Jan. 1999.

[5] Y. Li and L. J. Cimini, Jr., "Bounds on the interchannel interference of OFDM in time-varying impairments," *IEEE Trans. Commun.* , vol. 49, no.3, pp. 401-404, Mar. 2001.

[6] K. I. Lee, J. Kim and Y. S. Cho, "Computationally Efficient Signal Detection for STBC-OFDM Systems in Fast-Fading Channels," in *IEICE Transactions on Communications 2007,* vol. 90, no.10, pp. 2964-2968.

[7] J. W. Wee, J. W. Seo, K. T. Lee, Y. S. Lee and W. G. Jeon, "Successive Interference Cancellation for STBC-OFDM systems in a fast fading channel," in *Vehicular Technology Conference 2005.* Vol. 2,pp. 841-844.

[8] J. Kim, B. Jang, R. W. Jr. Heath and E. J. Powers, "A decision directed receiver for Alamouti coded OFDM systems," in *Vehicular Technology Conference 2003*.vol 1, pp.662-665.

[9] J. Kim,, R. W. Jr. Heath and E. J. Powers "Receiver designs for Alamouti coded OFDM systems in fast fading channels," *IEEE Trans. Commun.,* vol. 4, no.2, pp. 550-559,Mar., 2005.

[10] L. Deneire, P. Vandenameele, P. van der Perre, B. Gyselinckx and M. Engles, "A low-complexity ML channel estimator for OFDM," *IEEE Trans. Commun.,* vol. 51, no.2, pp. 135-140,Feb., 2003.

[11] J. H. Park, M. K. Oh and D. J. Park, "New Channel Estimation Exploiting Reliable Decision-Feedback Symbols for OFDM Systems," in *IEEE International Conference Communications, 2006.*, vol.7, pp. 3046-3051.

[12] M. L. Ku and C. C. Huang, "A refined channel estimation method for STBC/OFDM systems in high-mobility wireless channels," *IEEE Trans.Wireless Commun.,* vol. 7, no.11, pp. 4312-4320, Nov., 2008.

[13] M. L. Ku and C. C. Huang, "A derivation on the equivalence between newton's method and DF DFT-based method for channel estimation in OFDM systems," *IEEE Trans.Wireless Commun.*, vol. 7, no.10, pp. 3982-3987, Oct., 2008.

[14] T. A. Lin and C. Y. Lee, "Predictive equalizer design for DVB-T system," in *ISCAS 2005*, Vol. 2, pp. 940-943

[15] H. Hijazi and L. Ros, "Rayleigh time-varying channel complex gains estimation and ICI cancellation in OFDM systems," in *European Trans. on Telecommun. 2009*, vol.20, p p. 782-796.

[16] H. Hijazi and L. Ros, "Time-Varying Channel Complex Gains Estimation and ICI Suppression in OFDM Systems," in *IEEE GLOBECOM 2007*, pp. 4258-4262.

[17] H. Hijazi and L. Ros, "Polynomial estimation of time-varying multipath gains with ICI mitigation in OFDM systems," in *3rd International Symposium on ISCCSP 2008*, pp. 905-910.

[18] H. Hijazi and L. Ros, "Polynomial Estimation of Time-Varying Multipath Gains With Intercarrier Interference Mitigation in OFDM Systems," *IEEE* Trans.Vehic.Techno., , vol. 58, pp. 140-151, 2009.

[19] H. Hijazi, L. Ros and G. Jourdain, "OFDM Channel Parameters Estimation used for ICI Reduction in time-varying Multipath channels." in *European Trans. on Telecommun. 2007*.

[20] M. L. Ku, W. C. Chen, and C. C. Huang, "EM-based Iterative Receivers for OFDM and BICM/OFDM Systems in Doubly Selective Channels," *IEEE Trans. Wireless Commun.*,revised, 2009.

[21] A. Wenzler and E. Luder, "New structures for complex multipliers and their noise analysis," in *ISCAS 1995* , vol.2, pp. 1432-1435.